2001

# Towards a biochip for ion channel research

Santosh K. Pandey
*Lehigh University*

Pandey, Santosh K.

# TOWARDS A BIOCHIP FOR ION CHANNEL RESEARCH

June 2001

# Towards a Biochip for Ion Channel Research

by

**Santosh K. Pandey**

A Thesis
Presented to the Graduate Committee
of Lehigh University
in Candidacy for the Degree of
Master of Science
in
Electrical Engineering

Lehigh University
May 04, 2001

This thesis is accepted and approved in partial fulfillment of the requirements for the Master of Science

May 2nd 2001
(date)

Dr. Marvin H. White
Thesis Advisor

Dr. Bruce Fritchman
Chairman of Department

# Acknowledgements

At this point, I would like to express my sincere appreciation to my academic advisor, Prof. Marvin White. His help and guidance was always there whenever I needed it. He is the one whose foresightedness helped me to start with this project in the first place itself. The encouraging discussions I had with and the innovative ideas I received from Dr. Janet Robertson were also valuable for this project.

From my friends and colleagues' side, I would like to acknowledge the lively conversations and also the fun time I had with Jiankang Bu, Huiling Shang, Yu (Anne) Zeng and Steve Wrazien. Mrs. Linda Dreisbach deserves special thanks for providing administrative assistance to the research group. Mr. Ray Filozof was the person who showed me the different processing tools in our lab and also helped me a lot with my processing. Dr. Floyd Miller helped me with the AFM pictures. Mr. Bobby Hoogen from Agere Systems described his FIB system and helped me drill pores using the FIB system.

Finally, I would like to thank my parents for all the big and small things they did for me. The last (but not the least) note of thanks to some of my close friends: Abhi, Vspandey, Meikwan and Sooraj

# Contents

# List of Figures

**Figure 6.9:** Shows the inside surface of the well just 0.5-1 hour before the completion of the etching process. The residues and deposits here are also the etched silicon.

**Figure 6.10:** Shows the well after the etching process is completed. The residues and deposits are from the oxide, which is now being attacked by the KOH. After BHF dip these residues are no longer seen.

**Figure 6.11:** Shows the front side of the wafer, which has the nitride membrane resting on a 330μm deep well. The nitride appears to be transparent to light when seen under the optical microscope.

**Figure 6.12:** Shows the micropores drilled in the nitride membrane using the FIB system.

**Figure 6.13:** Shows a 4μm diameter circular hole etched in the nitride/oxide layer.

**Figure 6.14:** This AFM picture shows the 4μm hole chemically etched in the oxide/nitride layer. The hole is actually not that deep (around 1200A°) which is why the perception of the hole is not so distinct.

**Figure 6.15:** This AFM picture shows the texture of the surfaces after the hole was chemically etched in silicon. It can be seen that plasma etching (of the nitride) increases the surface roughness and chemical etching (of the oxide) after that still adds to the roughness.

# Abstract

This work describes the technology and techniques required for the fabrication of 'micro/nanopores' of varied shapes and sizes on a thin membrane resting on an ultra-deep silicon well (330μm). These micro/nanopores will become part of a unique planar 'nanopipette' for the study of single ion channels in biological cells. In the future, on-chip electronics will also be provided to amplify the low-level ion-channel signals in a greatly reduced noise environment. Although this 'Biochip' has applications in pharmacology, the same structure can be used for the rapid electronic sequencing of the individual bases in single-stranded DNA molecules by measuring ionic current changes as each nucleotide passes through a nanopore.

The fabrication of this interesting structure on silicon requires precise control of the different processing steps involved. Ultra-deep etching of silicon should give a well (~330μm deep) with smooth sidewalls and a thin nitride membrane (~800A°) resting on it. The membrane should not collapse during the process of drilling the pores in it or during the fluid-handling process. In the future, processing would involve not only the device fabrication but also the circuits and sensors fabrication on the same chip. In this work, the conditions and factors related to the fabrication of such a device are discussed with proper illustrations. The pores were drilled in the membrane using a Focused Ion Beam System. The results obtained from the experiments are very encouraging for future work on this project.

# Chapter 1
# Introduction

In this chapter we present the issues studied in this thesis and the motivation behind their study. We also discuss our objectives and present a brief outline of the thesis.

## 1.1 Motivation and Objectives

In addition to biological research, the study of cellular functions *in vitro* is basic to other fields such as clinical diagnostics, therapy, pharmacological drug screening and environmental monitoring. In this project, Biotechnology, Silicon Micromachining, Microelectronics and Circuit Analysis/Simulation are all merged to realize a test chamber for the examination of ion channels in biological cells. At present, the experimental testing and evaluation of the effect of drugs on ion channels is done using a unique glass micropipette and a measurement setup designed by Axon Instruments. It turns out that such an experimental setup becomes very noisy while recording very low currents (~pA). This might not pose a problem during 'whole-cell' recording when the current levels are pretty high (~nA) but is certainly not so satisfactory for measuring 'single-channel' currents. The commercial 'patch-clamp' amplifiers available today for amplifying the recorded low-level currents have adopted different designs to achieve higher bandwidth of operation and lower noise-level in the system. One such design is based upon an integrating front-end amplifier or 'headstage' where the noise is significantly lower and

the linearity is greatly improved. Even after adopting this integration-differentiation approach, these amplifiers are limited by several issues. The first issue is the long lead length between the ion-channel and the amplifier, which contributes to noise pickup. The second issue is the susceptibility of the head amplifier in present-day design to table vibrations, which leads to displacement currents in the output signal. The use of the glass micropipette limits the time resolution of the system, which is dependent on the pipette series resistance and the cell membrane capacitance. The micropipette has a series resistance as high as 10MΩ and so an extra series resistance compensation circuit is added in present-day measurement circuits.

In this project, we plan to build a device structure in silicon, which would basically perform the same function as the micropipette in the conventional cell-recording setup. The device would consist of a thin membrane resting on a well etched in silicon. A micro/nanopore would have to be drilled in the membrane and fluid chambers built on either side of the membrane. The electronics can be built on-chip next to the fluid chambers as well. Efficient circuit design for recording low-level currents can solve many problems associated with the conventional measurement technique. Because the device structure is planar, the series resistance is greatly reduced as compared to that of a glass micropipette. Integrating the electronics with the fluid chambers would provide a low-noise system, which is stable against mechanical vibrations. An added advantage would be the ease of bulk processing of such structures, which would now be cheaper, faster and far less noisy. Low-level signal recording is very challenging because of the contribution of noise from almost every component in the setup. In such cases, this

approach like ours that reduces noise, time constant and cost all at the same time is certainly very promising.

## 1.2 Thesis Outline

In this thesis we discuss the technology and techniques to fabricate a micro/nanopore in a thin membrane resting on a deep well etched in silicon. This will the first step towards making a Biochip, which has several advantages as compared to the present-day methods of cell measurements.

In Chapter 1, we discuss the motivation and objectives of this work, emphasizing the usefulness of building a planar micropipette in silicon.

In Chapter 2, we talk briefly about the history of the field of electrophysiology. This is followed by an introduction to electrophysiology with some cellular definitions and methods of cellular measurements.

In Chapter 3, we talk about the different processing steps involved in the fabrication of the proposed device in silicon.

In Chapter 4, the photomasks used for photolithography are shown.

In Chapter 5, we talk about the Focused Ion Beam System and the usefulness of this system for making our micro/nanopores.

In Chapter 6, the factors affecting ultra-deep anisotropic etching of silicon in aqueous KOH solution is discussed. Pictures are also shown for all the experiments conducted during the fabrication process.

# Chapter 2

# Electrophysiology

## 2.1 Brief Historical Note

By the end of the eighteenth century the notion that animal tissue both generated and responded to electricity was reasonably well established [1]. By the end of the nineteenth century, the Spanish histologist Ramon Cajal had demonstrated that the nervous system also consisted of individual cells called neurons [1]. Thus, the interpretation of the electrical properties of living tissues began to focus on the electrical properties of living cells. It was postulated that a cell consists of a semipermeable membrane surrounding an electrolytic interior. When the cell is at rest, an electric potential difference exists across the membrane, and the electrical activity recordable from such a cell consists of a change in this potential difference resulting from changes in membrane permeability. Techniques for extracellular recording of the activity of single cells led to the recognition that nerve fibers transmit information coded in the form of a temporal sequence of identical pulses called action potentials [1]. In the decade from 1940-1950, techniques were developed to record intracellularly, and it became possible to measure and/or control the potential across cellular membranes [1]. Since 1950, microelectrode-recording techniques have been greatly refined to enable intracellular recording from smaller cells [1]. A focus has been on determining the membrane mechanisms responsible for the generation

of electric potentials and on determining the effects of these potentials on other cellular processes. In the three decades beginning in 1960, microanatomical techniques, especially the development and routine use of the electron microscope, have enabled visualization of cellular and sub-cellular structure with much higher resolution [1]. Microchemical techniques have revealed information about the molecular constituents of cells [1]. Genetic engineering has enabled investigations of the relation between molecular constituents of parts of simple organisms and the behavior of whole organisms [2]. Microelectrophysiological techniques have been developed to measure the currents flowing through individual ionic channels [2]. Finally, the advent of the digital computer has greatly extended the ability of experimenters to quantify both anatomical and physiological measurements, and for theoreticians to develop conceptualizations of cellular systems. The aims of electrophysiology remain the same: to explain the electrical phenomena of living cells in molecular terms, and to explain the behavior of organisms in terms of the underlying cellular electrical processes [1].

## 2.2 Cellular terms

There is a difference of electric potential, maintained across the membrane of a living cell by the diffusion of ions across the cellular membrane, called the *resting potential*. This membrane potential changes in response to changes in numerous physiochemical variables, e.g. temperature, pH, extracellular concentration of ions, extrinsic electric current, etc. Electric potential changes are involved in many

cellular processes. However, electric potential changes have an additional important function. For neurons, electric potential changes are used to code information into the nervous system. In the nervous system, information comes in through the sensory organs that transduce the incoming mechanical, electrical, optic, or chemical signals into electric potential changes that are then processed to produce outputs that are primarily motor, but also secretary, photic or electrical. Electric potential changes function as a common currency for representation of information [1].

*Ion channels* consist of intrinsic membrane proteins that control the flow of specific ions across the hydrophobic barrier of a cellular membrane. They utilize the energy stored in chemical concentration gradients to produce small electrical signals during the movement of charged ions. Cells utilize this signaling for a wide variety of functions. Thus, ion channels are the molecular elements of excitability in nerve, heart and skeletal muscles and they regulate functions in numerous non-excitable cells as well. Our knowledge of the function of voltage-gated ion channels has expanded significantly through biophysical experiments carried out in the past few decades. *Patch clamp methods* have permitted analysis of individual ion channels in very small cells, which was not possible earlier [2]. Ion channels are named and classified primarily by their ion selectivity. Thus, potassium channels selectively allow passage of potassium ions to the exclusion of sodium, calcium and chloride etc.

## 2.3 New Electrical Recording Techniques

Prior to 1970s, intracellular electrical recording from single cells was

accomplished either via capillary electrodes inserted longitudinally into very large cells such as a giant axon of a squid or via micropipette electrodes used to penetrate cells transversely by puncturing the membranes. The penetrating micropipettes were widely used, but clearly had deleterious effects on small cells. During the 1970s and 1980s, new techniques were developed for recording from single cells and from isolated patches of cellular membrane that contained individual ion channels [2]. In the new technique, a micropipette, called a patch pipette, consists of a smooth (fire-polished) tip with a diameter of about 1μm placed in contact with a cell membrane as shown in Figure 2.1 below:

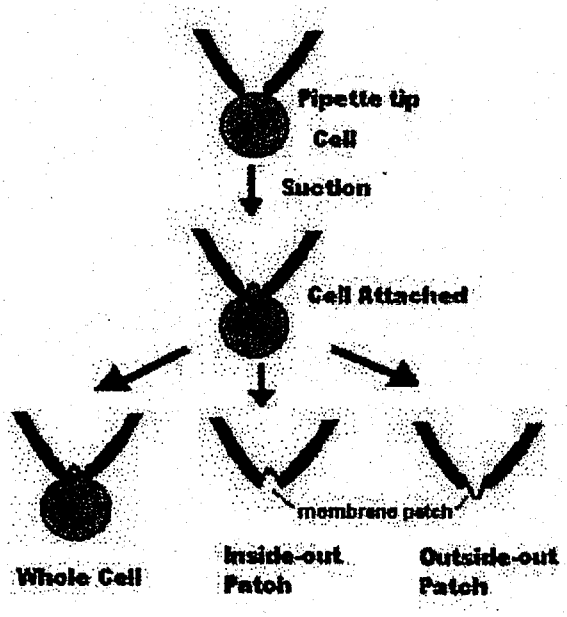


**Figure 2.1:** Illustration of the method for recording from cells and membrane patches.

If a slight suction is applied to the pipette, the glass seals to the cell with a very high-resistance seal (typically in the 10-100 GΩ range) so that current flow through the micropipette is confined to the patch of membrane in the tip of the pipette.

Electrical properties of this configuration, called the cell-attached configuration, have been recorded, but more useful results are obtained by further manipulations of the cell-attached configuration. The solution within the patch pipette exchanges fairly quickly with that of the cell; hence, the composition of the cytoplasm of the cell can be changed. The external concentration can be controlled by placing the cell in a bath of known composition. In this way, it is possible to study the membranes of relatively small cells and to approach the type of control of membrane electrical variables and solution compositions that was previously possible for very large cells. The tight seal between the patch pipette and the membrane reduces the incidence of large shunt leakage paths between the inside and the outside of the cell that are an important limitation of measurements with penetrating micropipettes. If the patch of membrane is separated from the cell, the resulting recording method is called the patch recording. In this method, a small patch of membrane, in one of two configurations – outside out or inside out – is lodged in the tip of the pipette. In an outside-out patch, the external surface of the membrane faces the outside of the pipette; in an inside-out patch, the cytoplasmic surface of the membrane faces the outside of the pipette. With either configuration, it is possible to control the concentration of the solution in the pipette and in the bath as well as the potential across the membrane in the tip of the pipette (Figure 2.2). The current through a single ionic channel in the patch can be measured under voltage clamp. This technique is called the patch-clamp technique [2-4].

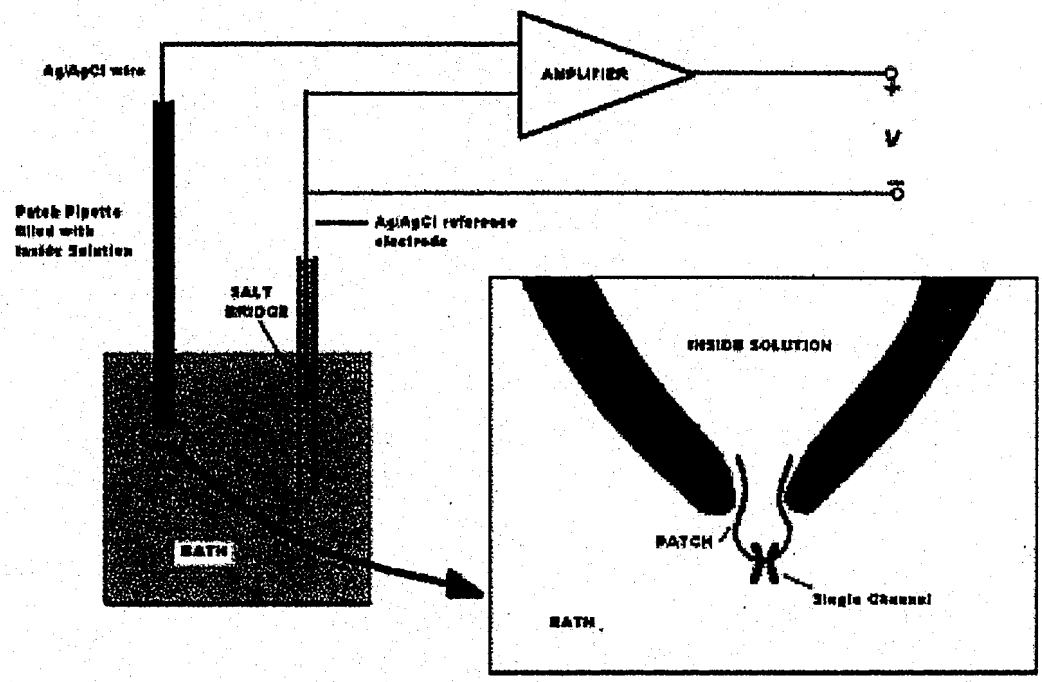


**Figure 2.2:** Illustration of the configuration of a pipette and a membrane patch.

Another experimental method to investigate ion channel function is known as the planar bilayer method. This is also a voltage-clamp method, but rather than employing glass electrodes to isolate and record channel behavior, a lipid bilayer membrane is incorporated onto a partition with a tiny hole. Ion channel proteins can be introduced into this bilayer, which effectively reconstitutes, in part, their membrane environment. In this method, electrodes placed in the fluid filled compartments on either side of the membrane are used to control the transmembrane electrical

potential and to monitor ion currents through the channels.

## 2.4 Macroscopic Ionic Currents

In the past it was recognized that the study of the membrane ionic current components under voltage-clamp conditions yielded important information about membrane mechanisms. Thus these voltage-clamp studies were refined and generalized in several distinct directions. We call these currents macroscopic currents to distinguish them from the single-channel currents that flow through single ion channels.

### 2.4.1 Selective Blocking of Channels by Pharmacological Agents

Pharmacological agents, often natural toxins known to affect electrically excitable cells, were applied to cells to determine which components of the membrane current were affected. Tetrodotoxin (TTX) [ref] and tetraethylammonim (TEA) [2] selectively block sodium and potassium currents, respectively. These agents have enabled investigators to block either the sodium current or the potassium current through the membrane in a reversible manner. Therefore, it has been possible to study the individual ionic currents more conveniently and selectively. More importantly, these studies indicated that not only are the mechanisms that give rise to the sodium and potassium conductances kinetically distinct, but they are also pharmacologically distinct. It was thus assumed that these conductances resulted from distinct structures in membranes, which came to be called channels.

### 2.4.2 Selectivity of Channels

It is important to know which ions permeate through each channel. It became clear that channels, though selectively permeable, could pass many ionic species. Thus, the sodium channel is a channel through which sodium normally permeates the membrane. Other ions also permeate through the same ion channel; however, there is a selectivity sequence. This selectivity is a characteristic property of a channel.

## 2.5 Single-Channel Currents

In the 1970s, Neher and Sakmann developed a method of recording currents through single ionic membrane channels [2-6]. This development revolutionized the study of ionic transport through membranes, and Neher and Sakmann were awarded the Nobel Prize for this development in 1991. With the single-channel recording method, it is possible to identify even those channels that are present at low density or that pass only low currents. Channels are categorized according to the identity of the physical variable, called the gating variable, that opens the channel, as well as by the ionic species that normally flows through an open channel. So, for example, channels that are opened by a change in the membrane potential are called voltage-gated channels, whereas channels that are opened by the binding of a ligand on the surface of the membrane are called ligand-gated channels, and so on. Thus, the voltage-gated sodium channel refers to a channel that is gated by a change in membrane potential and one that normally allows transport of sodium.

A principal finding is that single-channels have a discrete number of

states of conduction – often only one – when the channel is open and conducts transmembrane ionic current [2]. Channels have multiple closed or nonconducting states. A channel switches randomly between its open and closed states, with the probability of being in one state or another dependent upon the gating variable. A channel is formed by an integral membrane macromolecule that spans the membrane. The voltage-current characteristics of the channel are determined both by a gate that determines the extent to which the channel is opened or closed and by a selectivity filter that largely determines the current-voltage relation of an open channel (Figure 2.3). The average distance between channels can vary from 10nm to 1μm.

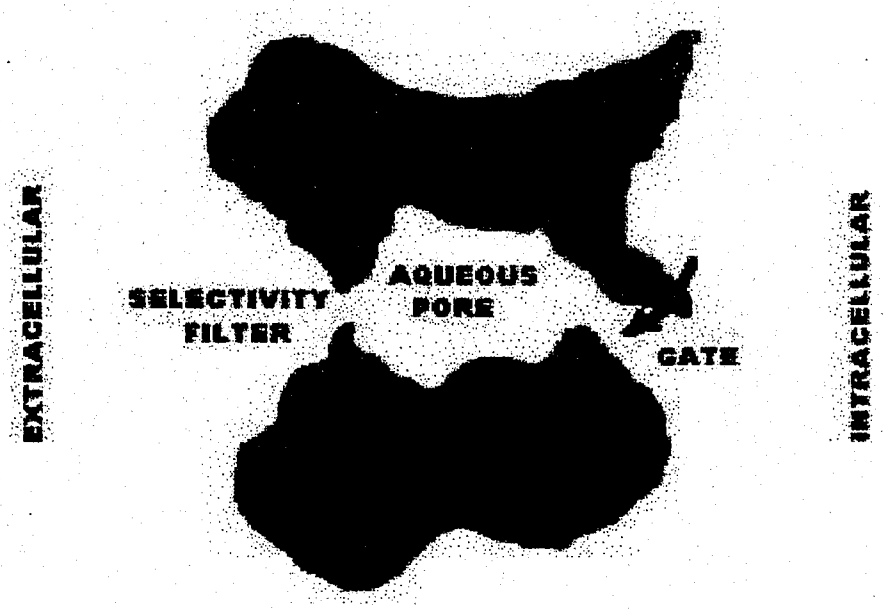


**Figure 2.3:** Schematic drawing of a hypothetical membrane ionic channel.

### 2.5.1 Ionic Currents in Single Channels

The single-channel current is not simply a scaled replica of the macroscopic current. In fact, single-channel currents exhibit rapid transitions between discrete conducting states. Most channels have one conducting or open state and multiple closed states. In the open state, current flows through the channel, and in the closed state it does not. The transitions between open and closed states are not only rapid, but they occur at random time intervals. The rates of transition among states depend upon the gating variable. So, for example, the voltage-gated sodium channel shows a larger probability of opening immediately after a depolarization and a larger probability of remaining open immediately after a depolarization. A change in the membrane potential across a single channel affects the single channel open-current magnitude for all single channels, whether they are voltage gated or not. For example, the magnitude of the current when the channel is open increases as the magnitude of the potential increases for the ligand-gated channels (Figure 2.4). However, the rate of the opening or closing of the channel does not change appreciably. For voltage-gated channels, the probability the channel is open also increases markedly as the magnitude of the membrane potential is increased (Figure 2.4).

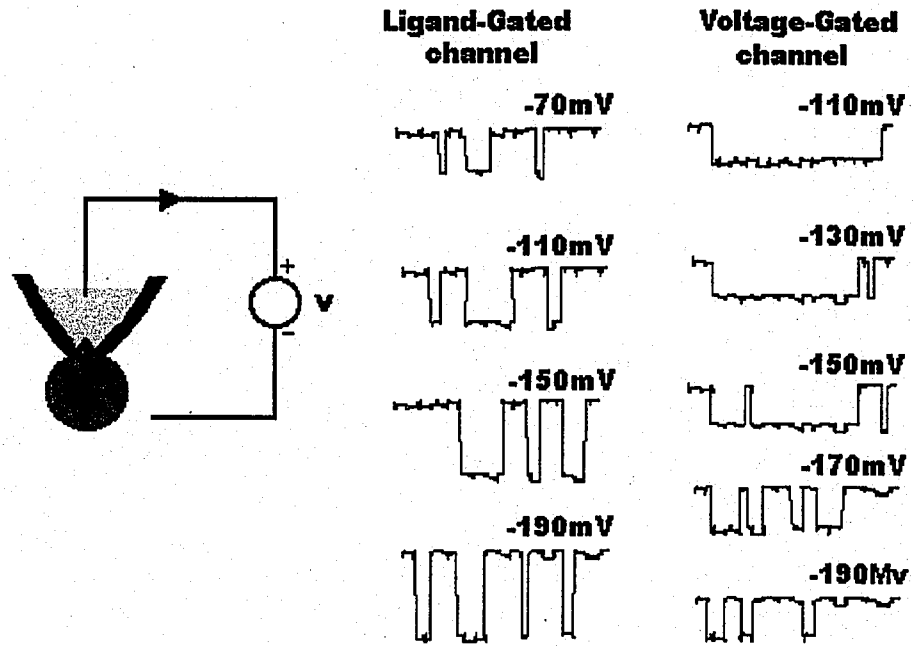


**Figure 2.4:** Measurements of currents through voltage-clamped patches of membrane in two different cell types of single channels.

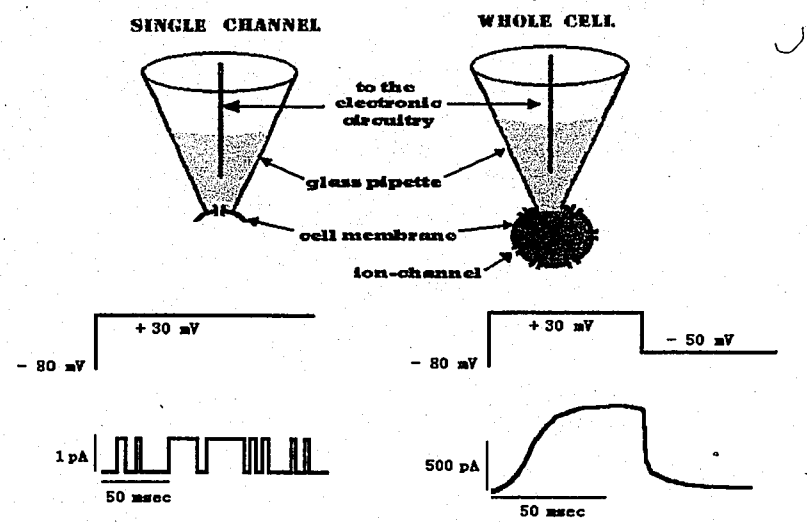


**Figure 2.5:** Illustration of the voltage-clamp technique, where the method on the right is called the 'whole-cell method (the entire cell surface is investigated). In contrast, on the left, a micropipette isolates a single channel in an excised membrane patch.

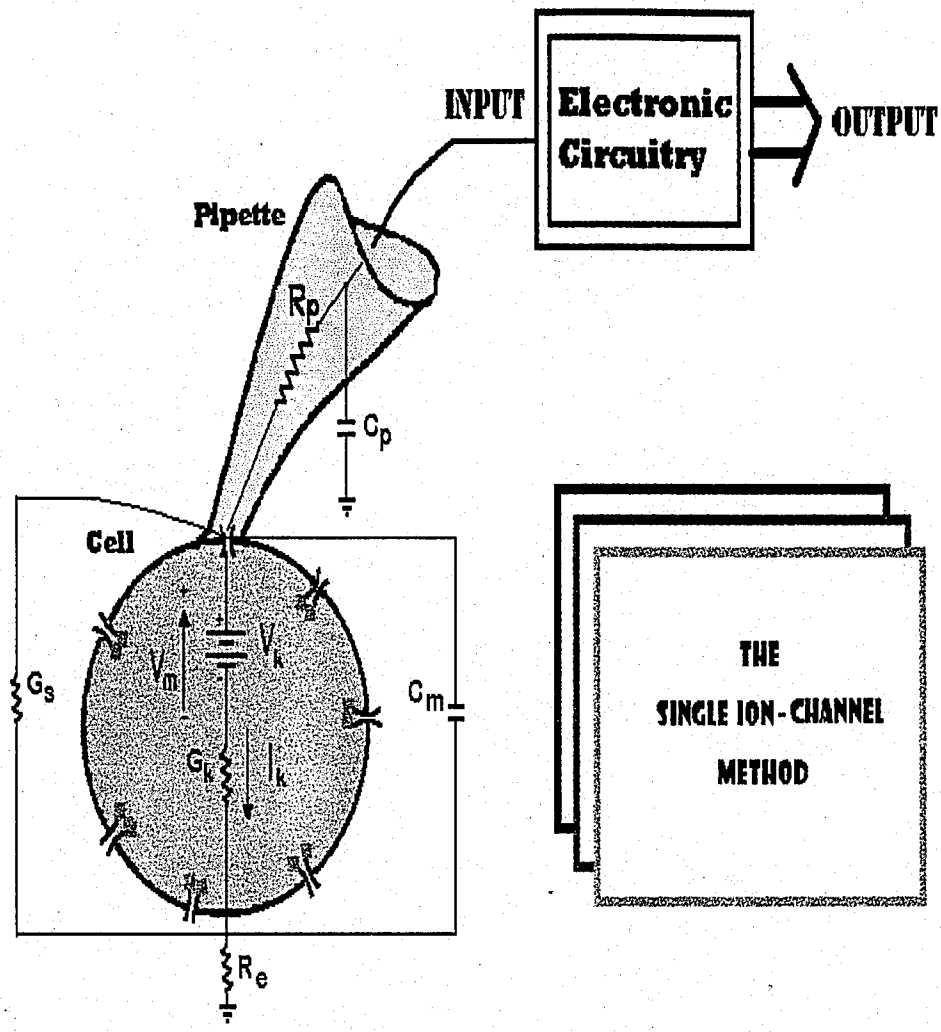


$$V_0(t) = -I_k(t) \otimes (1 - e^{-\frac{t}{r_p C_m}}) \frac{C_1}{C_F} R_1 \quad Integrating\ Front-End$$

$$V_0(t) = -I_k(t) R_F \qquad \text{Re}sistive\ Front-End$$

**Figure 2.6:** The Whole-Cell Method and an electrical model for the setup [4].

## 2.6 DNA sequencing using a Biochip

The Deoxyribonucleic acid (DNA) molecule contains all the instructions to make and sustain living organisms. DNA consists of two polynucleotide chains (strands) composed of four types of nucleotides subunits (bases). These strands are held together by hydrogen bonds to form a double helix. We can obtain all of the information required to determine the structure and function of an organism by reading the sequence of bases in a DNA strand. This is the driving force behind the considerable effort to sequence the genomes of various organisms, most notably that of humans. Researchers at Harvard and National Institute of Science and Technology (NIST) have suggested a method to rapidly sequence individual bases in a single-stranded DNA molecule by measuring the ionic current changes as each strand passes through a nanopore, which is sized to admit only a single strand [7,8]. Protein molecules span the lipid bilayer and act as ion channels (through a charge-controlled gating mechanism) to allow or block the flow of ions through the bilayer. A negatively charged, single-strand, DNA was drawn through these channels into a positively filled chamber. In the process, researchers suggested a 'stepped' ion current, corresponding to the passage of base diameters, may be measured in a detectable manner [7-11]. In order to accomplish the resolution required to measure these changes in ion current, we are working on a BioChip with integrated nanoscaled chambers, voltage amplifiers and sensors to resolve the current pulses in a low-noise environment [12,13].

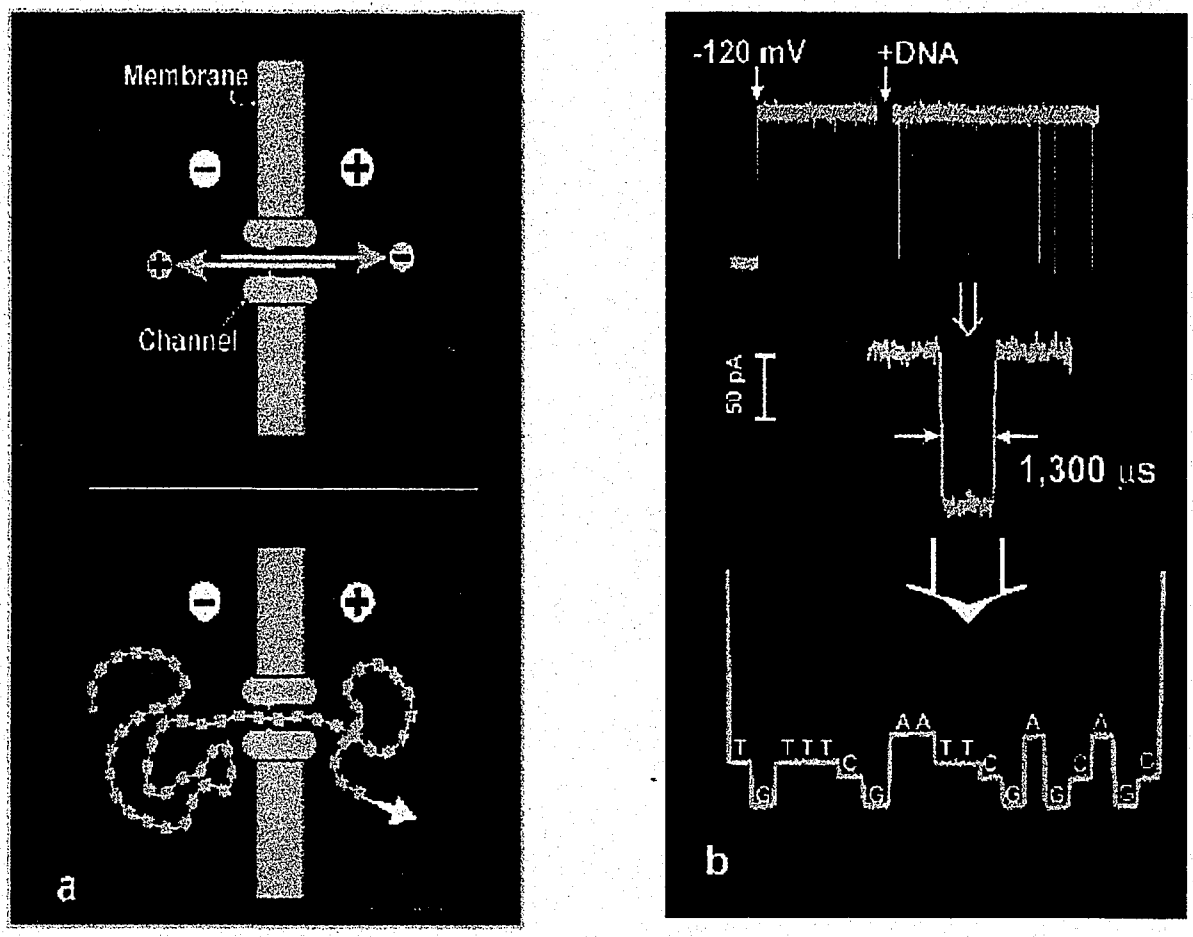


**Figure 2.7** (on the left) shows the basic principle of passing a DNA strand through a nanopore. The DNA strand is negatively charged and it can be pulled through the nanopore by applying a positive voltage at the other side of the nanopore [12].

**Figure 2.8** (on the right) shows the ion currents recorded when the DNA strand passes through the nanopore [12]. The conceptual illustration of the passage of a nucleotide is shown in the last figure.

# Chapter 3

# Silicon Processing

## 3.1 Processing Steps:

- Wet, thermal Oxidation at 1000°C for 60 minutes (1200A° of oxide)

- LPCVD Silicon Nitride Deposition at 800°C for 65 minutes (1200A° of nitride)

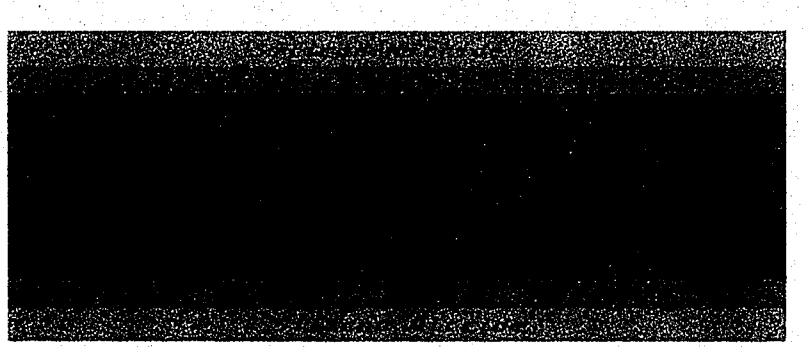

- Plasma Etching of the Silicon Nitride for 300 seconds, which takes away all the nitride at the backside and approximately 200A° from the front side.

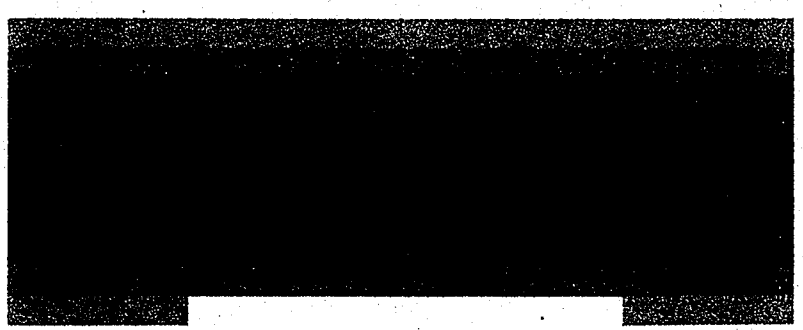

# Chapter 3

# Silicon Processing

## 3.1 Processing Steps:

- Wet thermal Oxidation at 1000°C for 60 minutes (1200A° of oxide)

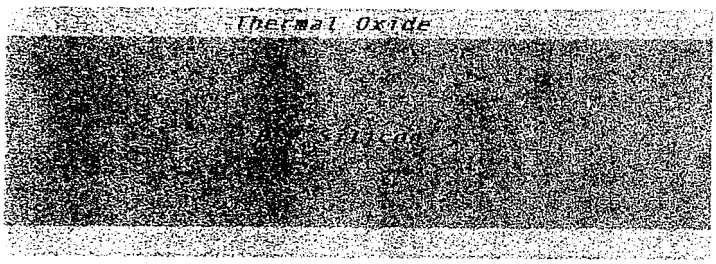


- LPCVD Silicon Nitride Deposition at 800°C for 65 minutes (1200A° of nitride)

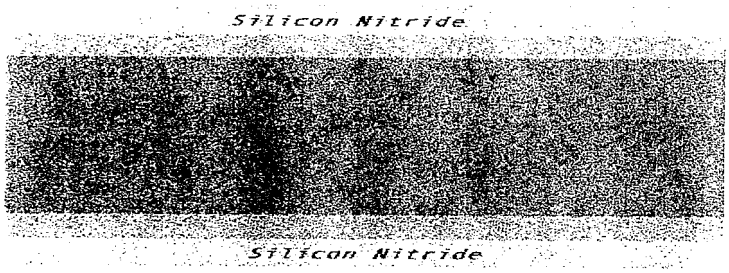


- Plasma Etching of the Silicon Nitride for 300 seconds, which takes away all the nitride at the backside and approximately 200A° from the front side.

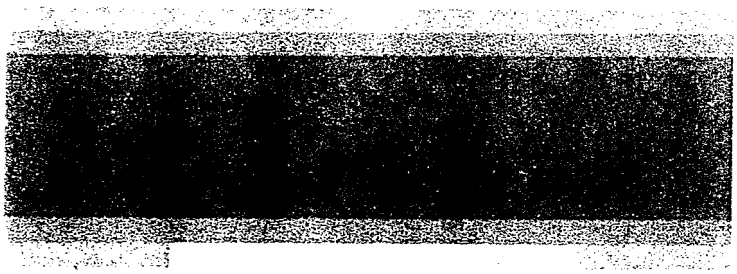

- Buffered HF dip of the wafer for 5 minutes to remove the oxide from the backside. The silicon nitride on the front side is relatively unaffected by the buffered HF solution.

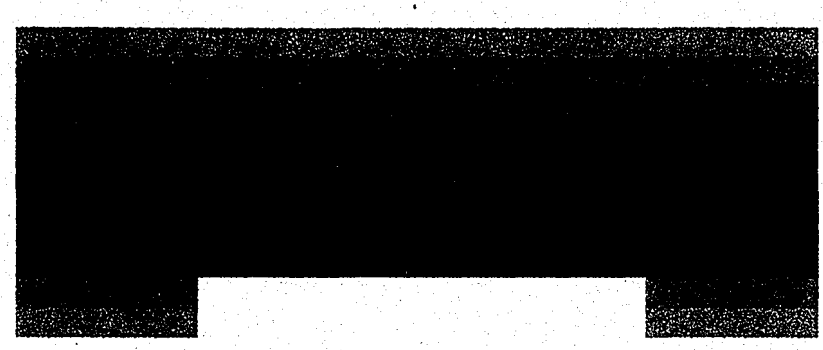

- Silicon etching in 20% KOH at 80°C for 6 hours.

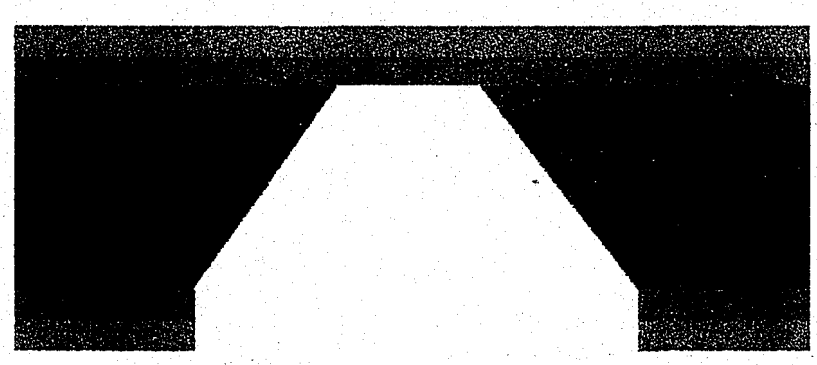

- Buffered HF dip of the wafer (5minutes) to remove the oxide below the nitride.

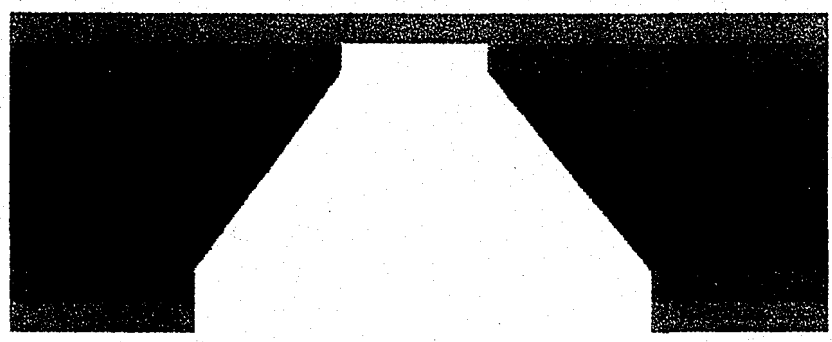

- Buffered HF dip of the wafer for 5 minutes to remove the oxide from the backside. The silicon nitride on the front side is relatively unaffected by the buffered HF solution.

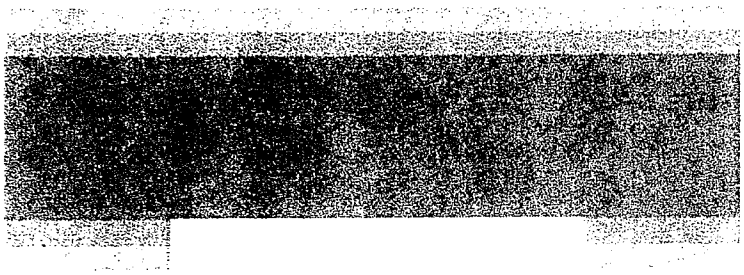

- Silicon etching in 20% KOH at 80°C for 6 hours.

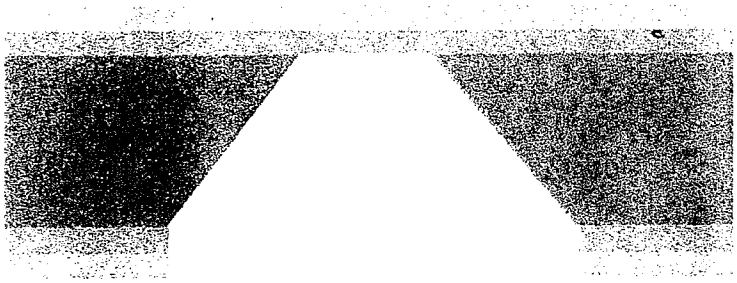

- Buffered HF dip of the wafer (5minutes) to remove the oxide below the nitride.

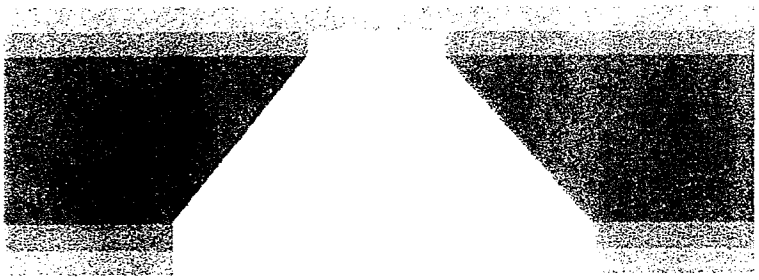

- Micro/Nanopores drilled through the nitride membrane using FIB.

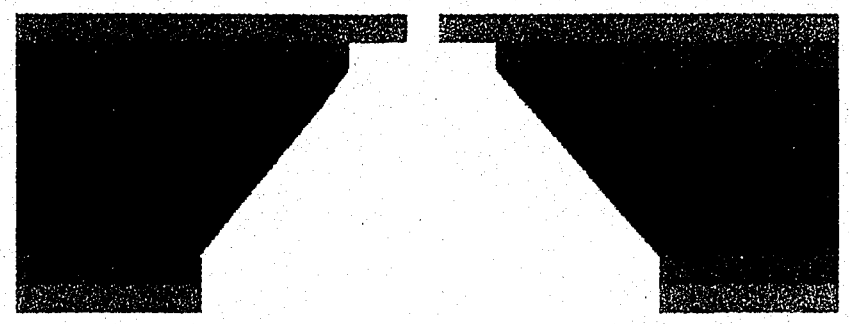

- LPCVD Silicon Oxide Deposition at 800°C for 30 minutes. (300A° of oxide)

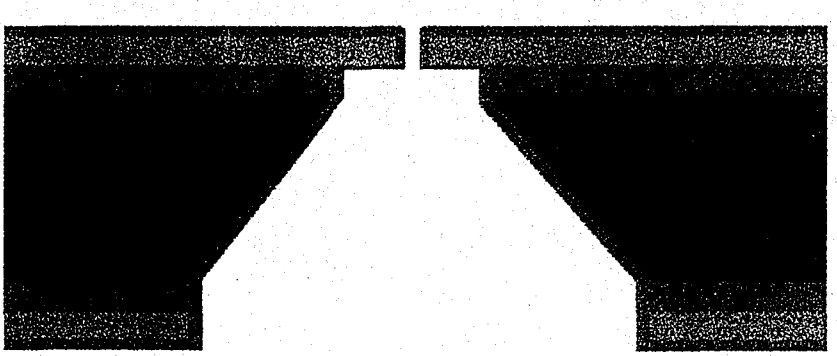

- Metallization at the backside to give the back electrode.

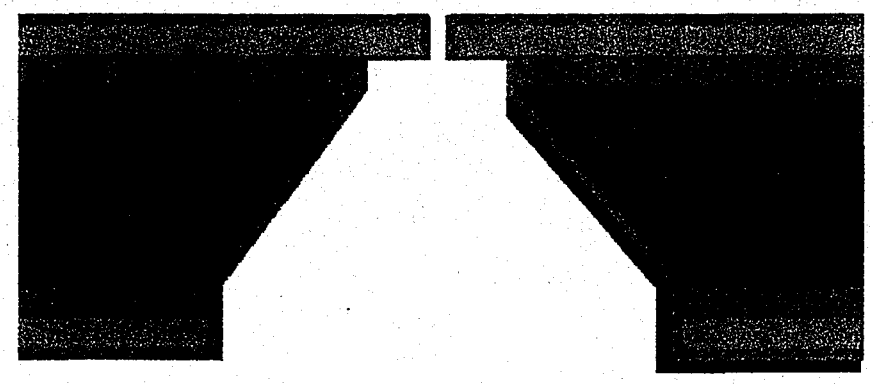

- Micro Nanopores drilled through the nitride membrane using FIB.

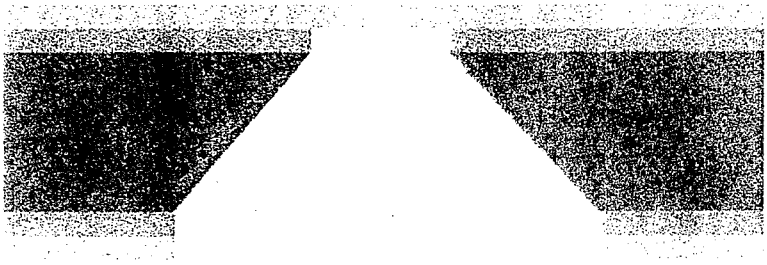

- LPCVD Silicon Oxide Deposition at 800°C for 30 minutes. (300A° of oxide)

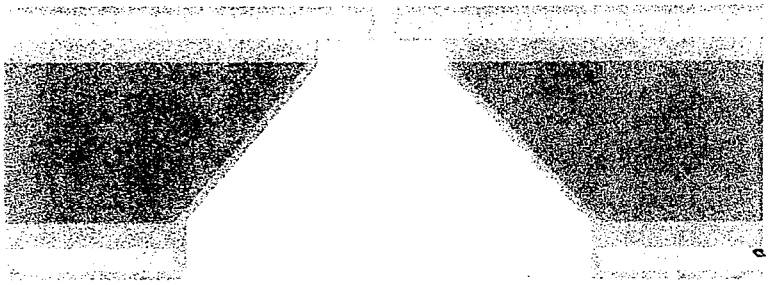

- Metallization at the backside to give the back electrode.

- SU-8 deposition to form the fluid chambers.

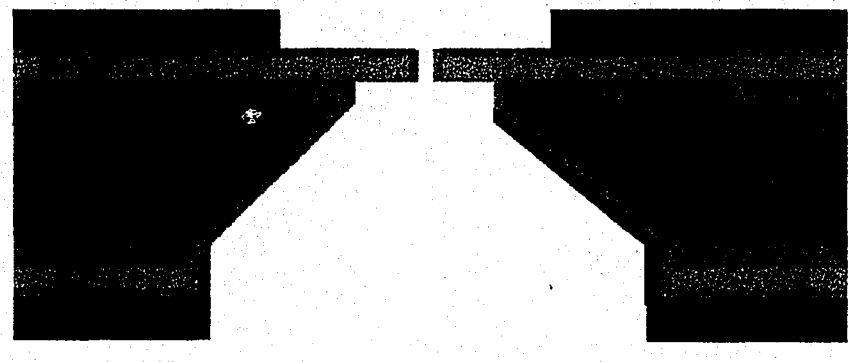

- Metallization at the front side to give the front electrode.

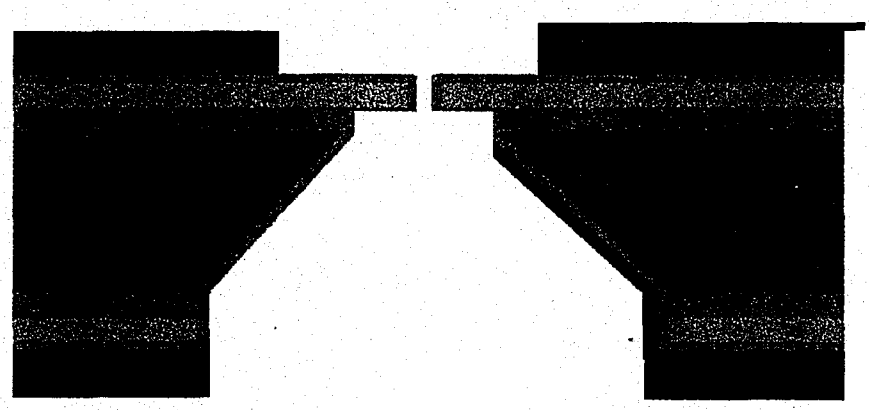

- SU-8 deposition to form the fluid chambers.

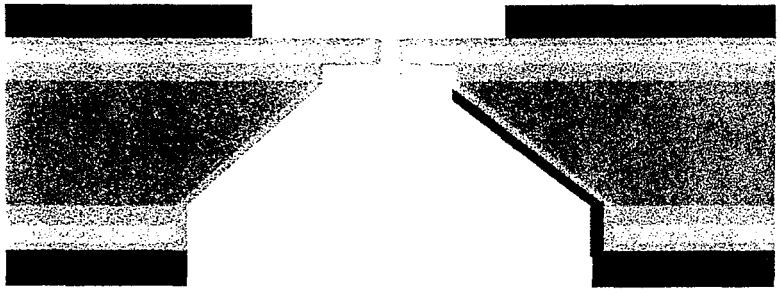

- Metallization at the front side to give the front electrode.

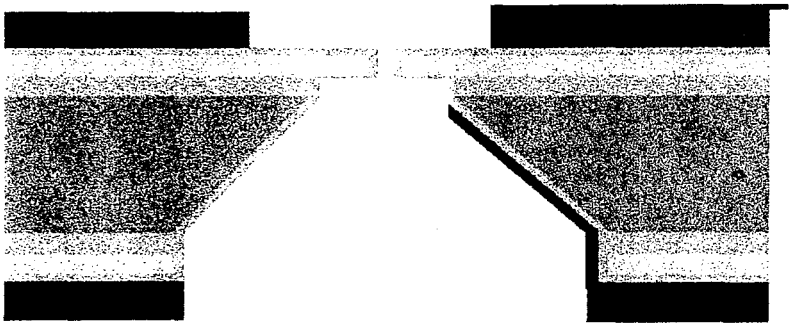

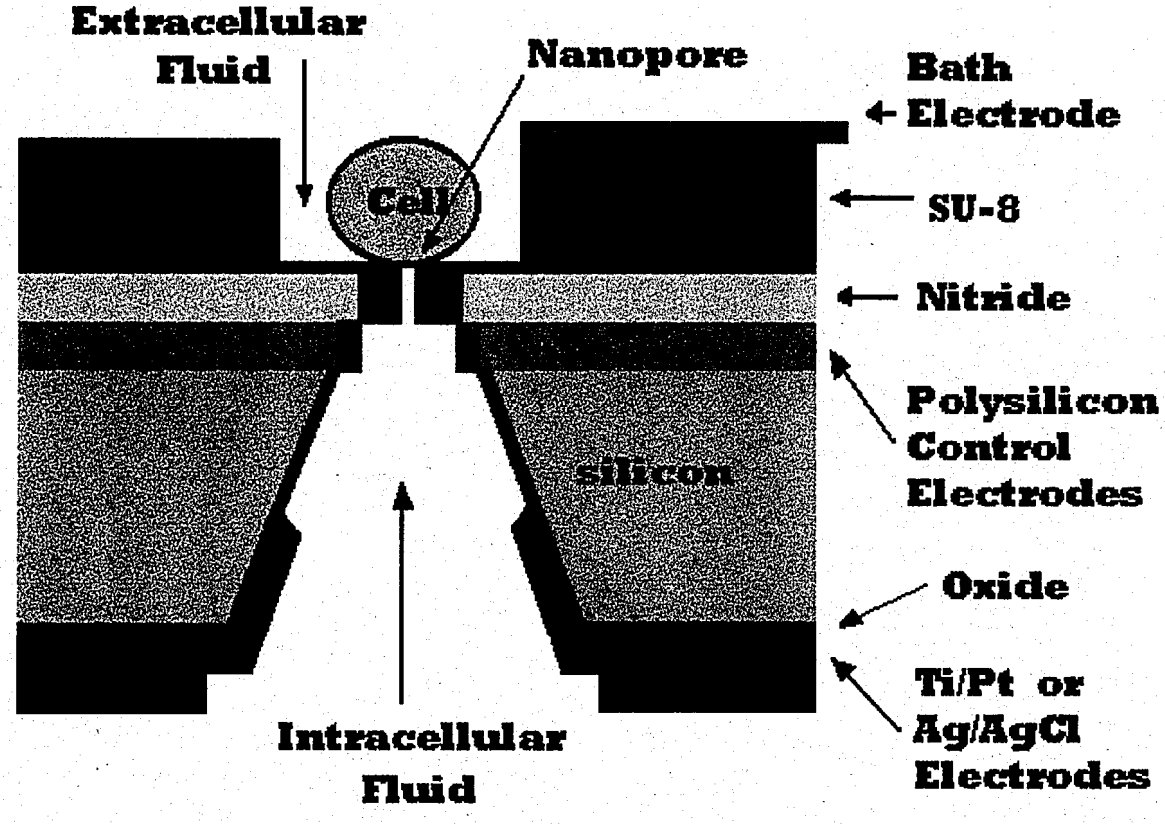


**Figure 3.1:** Final Device Structure with the cell

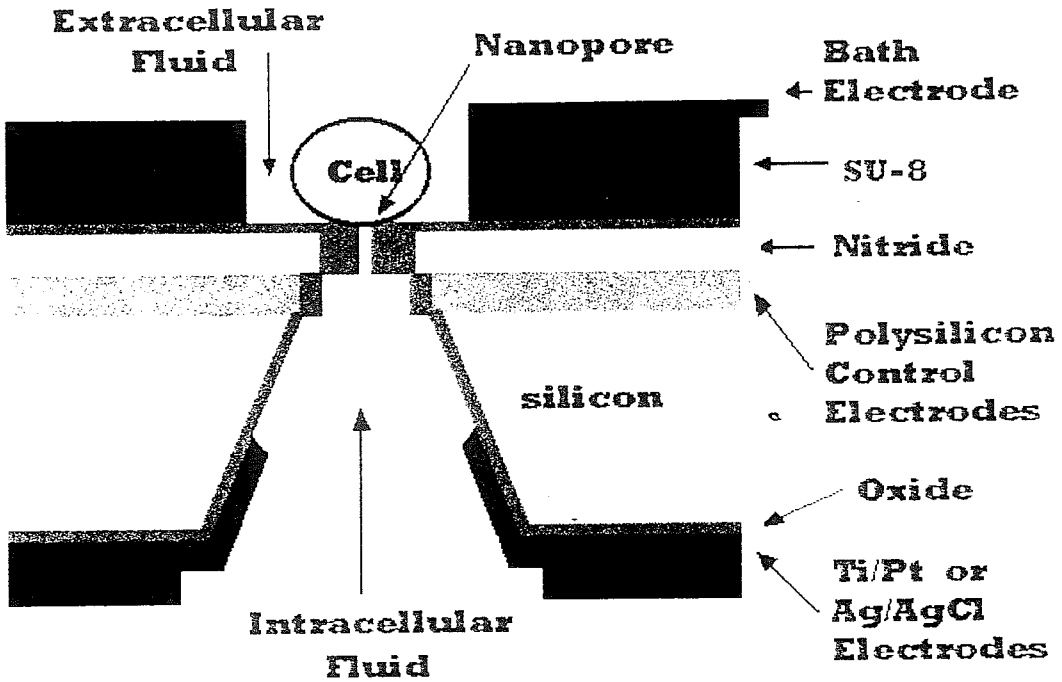


Figure 3.1: Final Device Structure with the cell

# Chapter 4

# Design of Photomasks

## 4.1 Photomasks

The masks for the processing were designed using MAGIC software available in the Display Research Laboratory of the Sherman Fairchild Laboratory. I designed two photomasks: one for the wells to be etched in the silicon and the other for the micropores to be etched in the nitride membrane. Actually, there are a total number of five masks required for the entire process:

- One for the wells in silicon.
- One for the back electrode metallization.
- One for the SU-8 deposition on the backside of the wafer.
- One for the front side deposition of SU-8.
- One for the front electrode metallization.

In the design of the photomasks, I planned preliminary experiments of silicon etching couple with the use of a Focused Ion Beam (FIB) to drill micro/nanopores in the nitride membrane. In the experiments to follow, I plan to design and use all the five photomasks mentioned above. However, this thesis will describe experiments using only two of the five photomasks. The structures fabricated in this thesis do not have SU-8 depositions or electrode metallizations, but they do show the feasibility of making micro/nanopores in a nitride membrane as thin as 800A°.

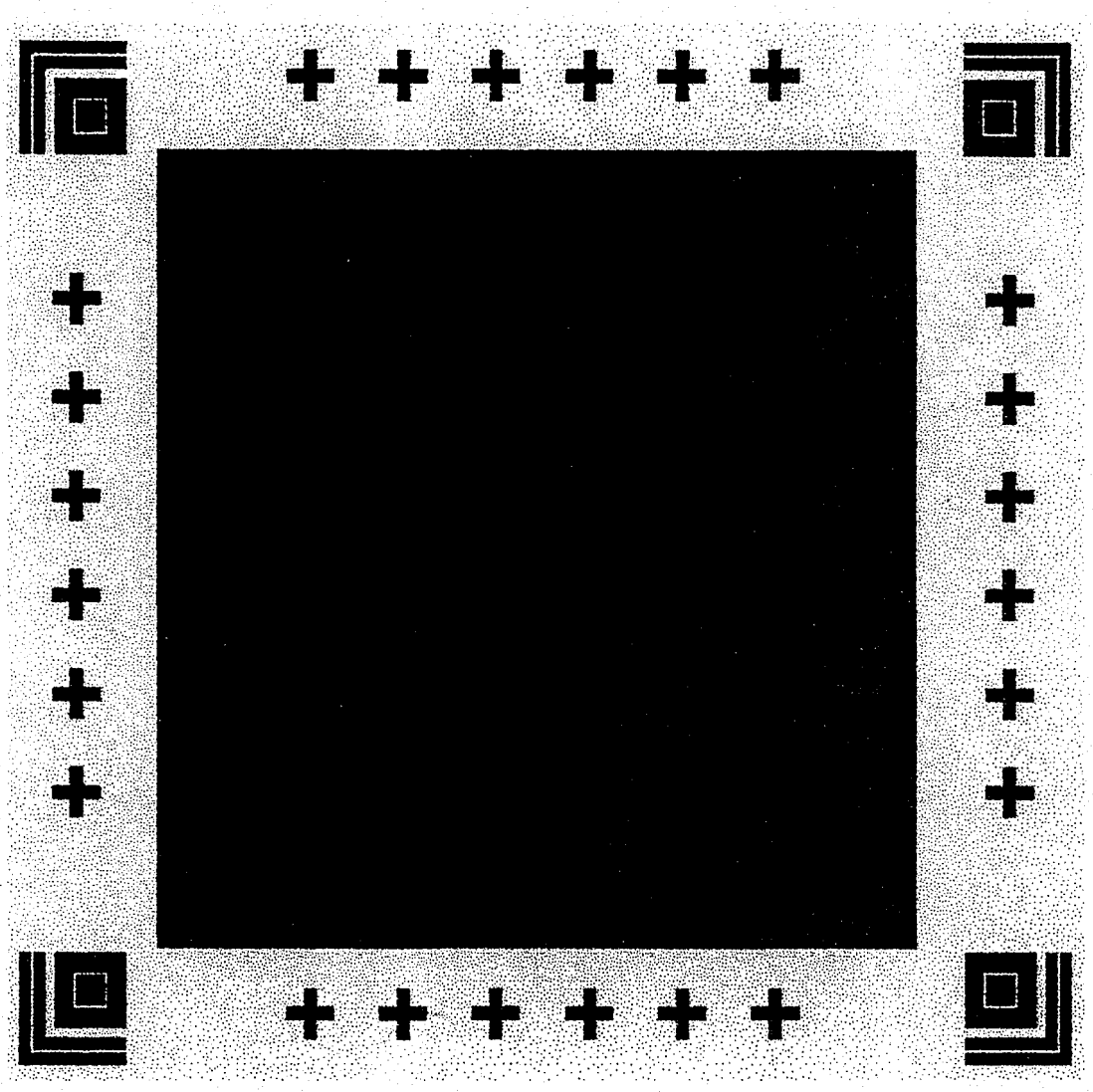

**Figure 4.1:** This figure shows the design of the two photomasks used. The first photomask is a square of size 650μm x 650μm. The alignment marks are shown on the sides of the square. Inside this big square can be seen a number of dark holes of varying sizes (4μm-7μm), which is the second photomask used.

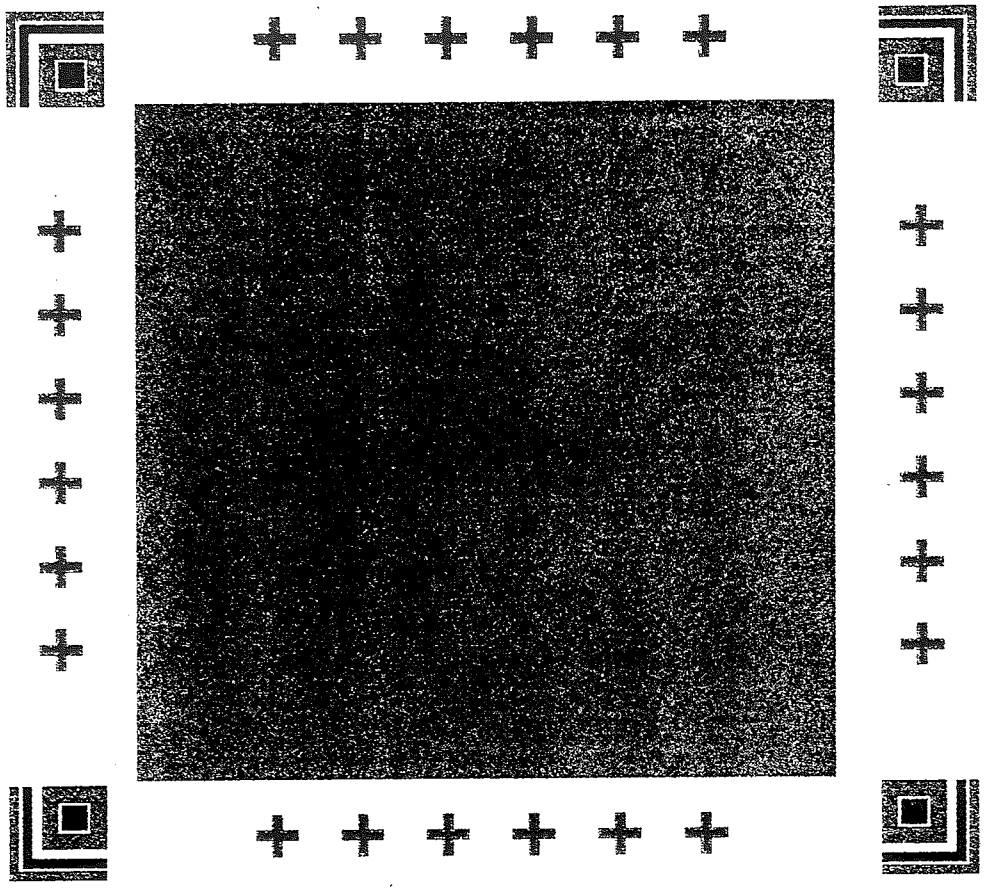

**Figure 4.1:** This figure shows the design of the two photomasks used. The first photomask is a square of size 650μm x 650μm. The alignment marks are shown on the sides of the square. Inside this big square can be seen a number of dark holes of varying sizes (4μm-7μm), which is the second photomask used.

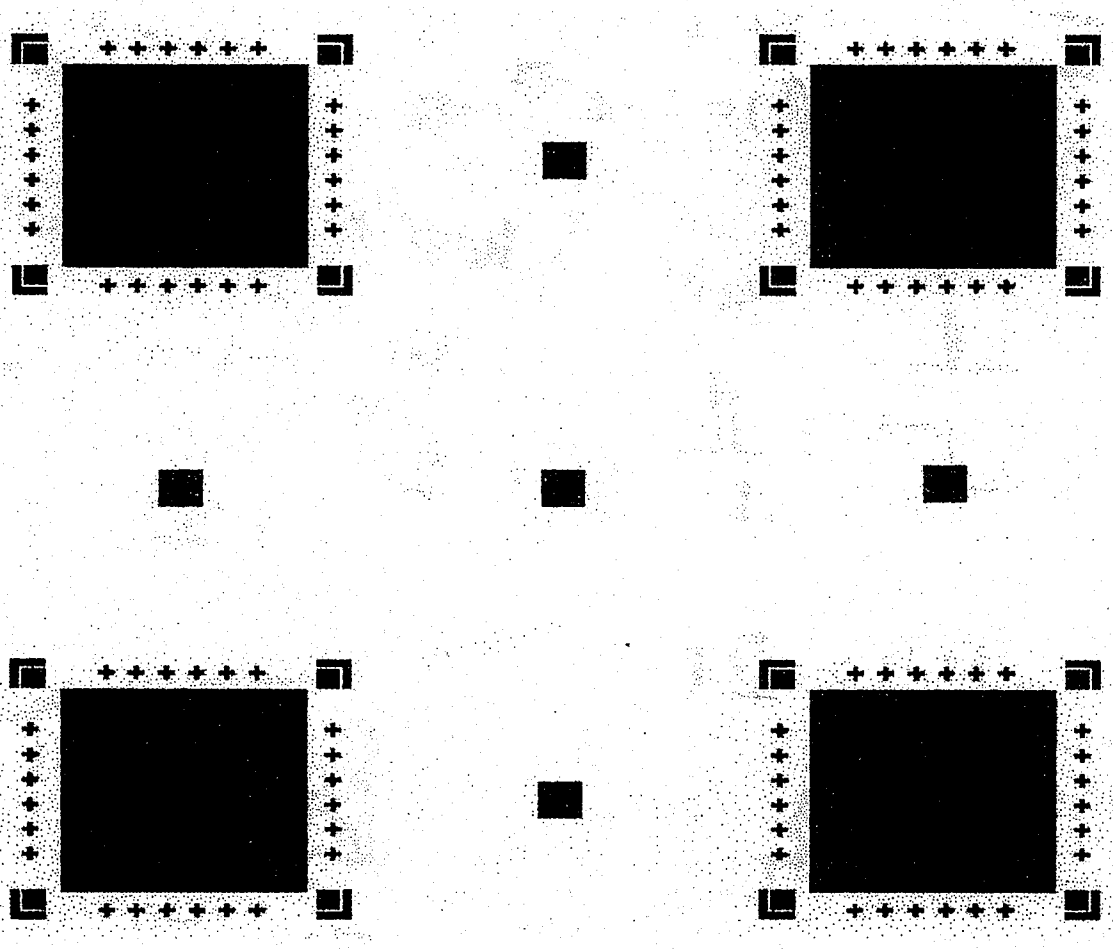

**Figure 4.2:** This figure shows one die in the photomask used. There are some more alignment marks in the center of the die for front-to-back alignment. The size of each die is 3000μm x 3000μm.

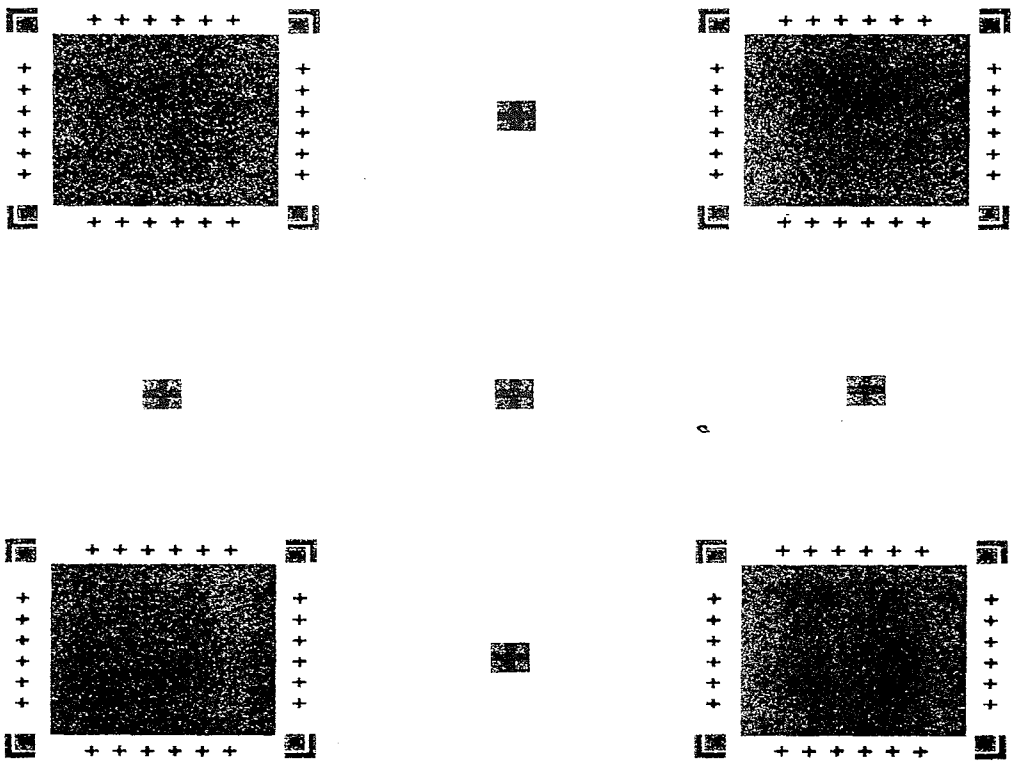

Figure 4.2: This figure shows one die in the photomask used. There are some more alignment marks in the center of the die for front-to-back alignment. The size of each die is 3000μm x 3000μm.

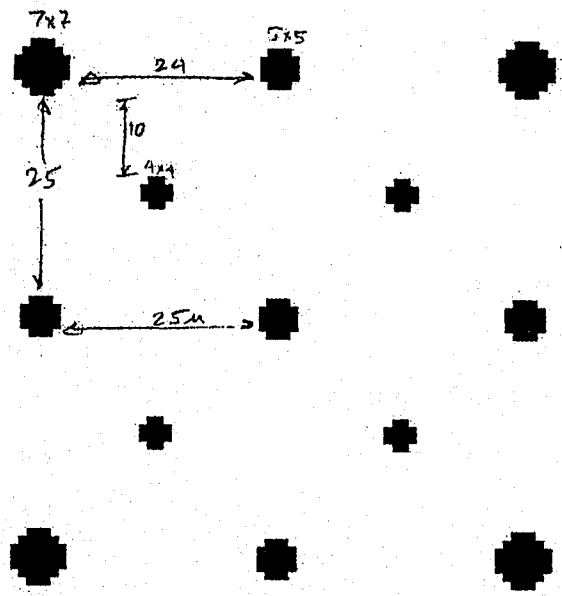


**Figure 4.3:** This figure shows the second photomask used for etching micropores of sizes from 4μm x 4μm to 7μm x 7μm. Smaller pores (even in the nanoscale range) were made using the FIB system.

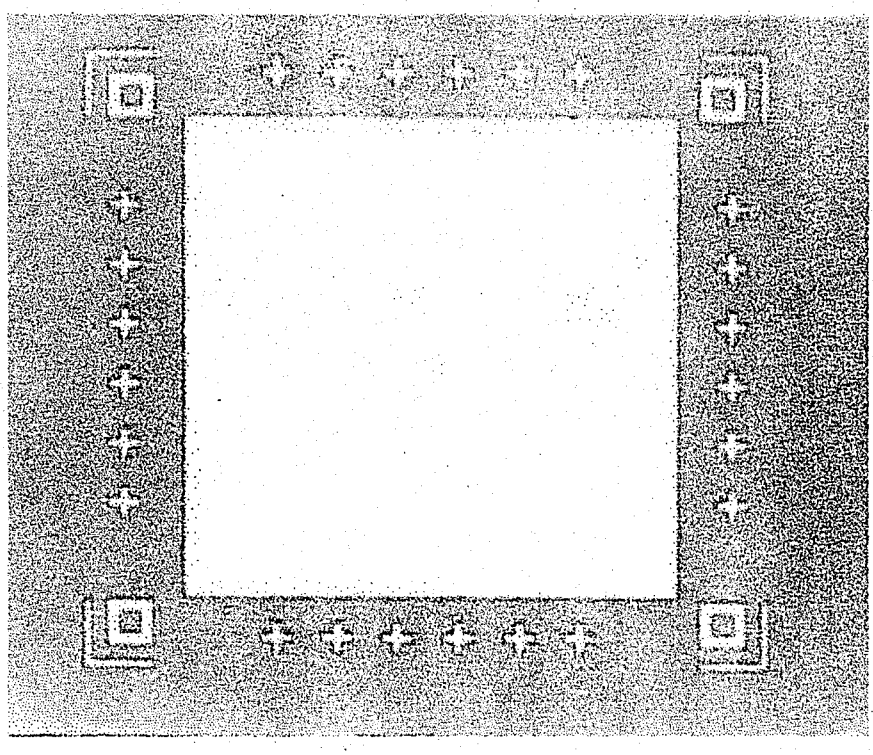

**Figure 4.4:** This figure shows the backside of the wafer after etching the oxide and the nitride from the backside to make the wells in silicon.

# Chapter 5
# Focused Ion Beam System

## 5.1 Focused Ion Beam technology

Ions of kiloelectron volt energies incident on a solid surface produce a number of effects: several atoms are sputtered off, several electrons are emitted, chemical reactions may be induced, atoms are displaced from their equilibrium positions, and ions implant themselves in the solid, altering its properties [14,15]. Some of these effects, such as sputtering and implantation are widely used in semiconductor device fabrication and in other fields [16-18]. Thus, the capability to focus a beam of ions to submicrometer dimensions (i.e. dimensions compatible with the most demanding fabrication procedures), is an important development. The focused ion beam field has been spurred by the invention of the liquid metal ion source and by the utilization of focusing columns with mass separation capability. This has led to the use of alloy ion sources making available a large menu of ion species, in particular dopants of Si and GaAs. The ability to sputter and to also induce deposition by causing breakdown of an adsorbed film has produced an immediate application of focused ion beams to photomask repair. The total number of focused ion beam fabrication systems in use worldwide is about 35, about 25 of them in Japan [15]. In addition, there are many simpler focused ion beam columns for specialized applications [19-21]. The interest is growing rapidly. The following range of specifications of these systems has been reported: accelerating potential 3 to 200kV, ion current density in focal spot up to $10A/cm^2$, beam diameters from 0.05 to 1μm, deflection accuracy of the beam

over the surface 0.1μm, and ion species available Ga, Au, Si, Be, B, As, P etc. Some of the applications, which have been demonstrated or suggested, include: mask repair, lithography (to replace electron beam lithography), direct, patterned, implantation doping of semiconductors, ion induced deposition for circuit repair or rewiring, scanning ion microscopy, and scanning ion mass spectroscopy.

## 5.2 Focused Ion Beam Machinery

A focused ion beam system can be thought of as composed of three main parts: the source of ions, the ion optics column, and the sample displacement table. A detailed understanding of these parts is too intricate for the scope of this thesis. Instead the principles of operation will be discussed briefly [15].

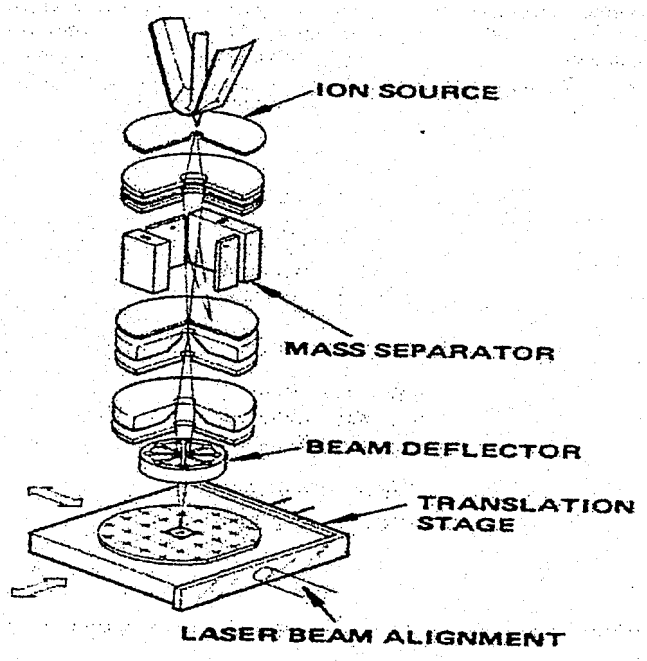


**Figure 5.1:** Schematic of a focused ion beam system including the source, column and the sample stage. The series of concentric electrodes between the source and the mass separator and between the mass separator and the beam deflector are electrostatic lens [15].

### 5.2.1 Source

The generation, deflection, and the focusing of ions have close analogies to optics. Thus, to illuminate a small spot with a large flux a 'bright' source of ions is needed with one or more 'lenses' between the source and the spot. Liquid metal field ionization sources are used to emit ions in the focused ion beam systems. In these sources a reservoir of liquid metal is maintained at one end of a sharp (usually tungsten) needle. The metal wets the needle and flows down to the tip. The tip of the needle faces an extraction aperture, a round washer like electrode concentric with the tip and some distance below it. A voltage is applied between the tip and the aperture. The electric field is highest at the tip and as a result the liquid metal is pulled into a sharp cone and ions are emitted from the tip of this cone. The radius of the tip has been measured to be less than 100 Angstroms. The liquid metal can be of any composition as long it wets the needle, does not corrode it, and has a low vapor pressure in the molten state. The list of elements that have been incorporated into ion sources is quite extensive [20]. The most commonly used ion is gallium since it is almost liquid at room temperature and yields a long lifetime source. The limit of the liquid metal field ionization source performance is largely determined by the electrostatic repulsion of the ions. Even though the diameter of the tip of the cone is about 100 Angstroms, the emission appears to be taking place from a 'virtual source' of 500-1000 Angstroms. The origin of this increase in effective size is due to the mutual repulsion of ions, which results in a spread $\Delta E$ full width at half-maximum in the energy of the ions (E) that finally arrive at the sample. This energy spread results in chromatic aberration.

### 5.2.2 Column

#### 5.2.2.1 Ion Column.

The column, which focuses ions from the source onto the sample, is very much analogous to a series of optical lenses, which may focus a source of light in one plane onto another plane. In electron beam lithography machines, the lenses often use magnetic fields to bend the path of the electrons. For ions this is not usually practical. The higher fields needed would be difficult to generate, since the ions are more massive and travel more slowly. Ion lenses are for most part electrostatic and consist of two (or more) very precisely machined washer-shaped electrodes at some higher potential. The beam passes through the center of these concentric electrodes and is deflected and accelerated by electric fields. The most serious practical limitation to the performance of most present focused ion beam columns is chromatic aberration. Spherical aberration is another effect that may increase the beam diameter.

#### 5.2.2.2 Mass Separator

Low melting point metals like Ga, In, or Sn can be liquefied in a source as discussed above. Other desired species such as Si, Be, B or As are incorporated into alloys which can operate in a liquid metal ion source. However, in such instances several species of ions are all emitted by the source. Mass separators using crossed electric and magnetic fields (ExB) are used in such systems. The principle of operation of the (ExB) mass filter is shown below. Strictly speaking, it is a velocity filter, but, since all ions arriving at the filter have been accelerated through the same potential,

ions of different mass or charge will have different velocities. The condition for passing through the filter undeflected is E=vB where E is the electric field, B is the magnetic field and v is the velocity.

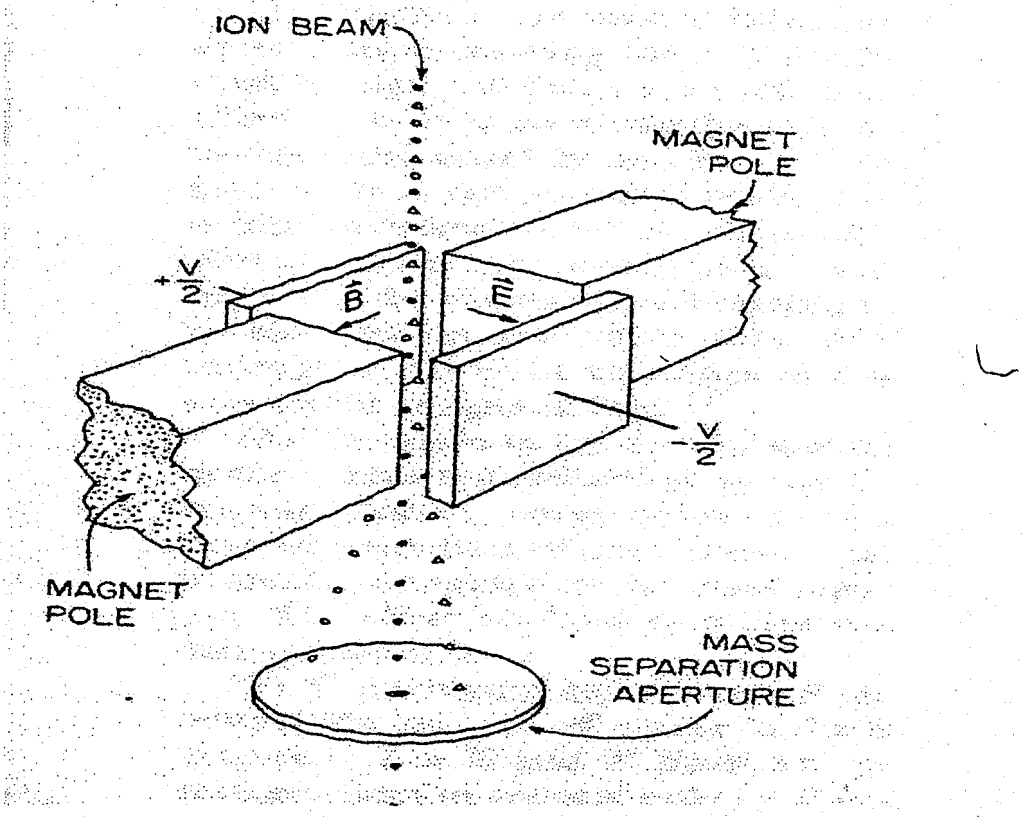


**Figure 5.2:** Schematic of mass separator with a beam of three species of ions (represented as solid, open circles and triangles)[15].

### 5.2.2.3 Beam Blanking and Deflection

A focused ion beam which is to be used for beam writing over selected areas need a beam blanker, i.e., means of turning the beam off. This is generally done by having a pair of electrodes on opposite sides of the beam and applying a voltage -Va/2 and +Va/2 to them, so that the beam is deflected sideways and is not capable of passing through an aperture located downstream. If the beam writing is to be

done at high speeds so that the beam is switched on at a given pixel for only 10-1000ns, then the blanker must turn the beam on at an even higher rate.

#### 5.2.2.4 Beam Profile

The ultimate resolution of any patterning done with focused ion beams will depend on the beam profile. The current density in the ion beam spot focused on a sample is thought of to have a Gaussian profile. However, detailed measurements have shown that about 2-3 orders of magnitude below the peak the beam profile deviates from a Gaussian and shows wider skirts.

### 5.2.3 Sample Stage

We have discussed the main elements, which make up an ion column. This ion column can focus a beam down to a 0.1μm spot or less and deflect this spot accurately and rapidly over a field typically 100-500μm in width and height. If we wish to address a larger sample (say, 5-in diameter), then a stage is needed to position the sample precisely under the beam while maintaining it in the focal plane. This capability has been well developed for e-beam lithography. The central element is a laser interferometer, which measures the position of the stage to an accuracy of 0.01μm. There are other elements included to control the movement and the speed of the stage.

## 5.3 Applications

A focused ion beam (FIB) is a very attractive tool in lithography, etching, deposition and doping. FIB technology is now used in various device processes and FIB etching and deposition has become indispensable in such fields as failure analysis, mask repair and TEM sample preparation [16,17,20,21].

### 5.3.1 Lithography

FIB lithography provides a new means of producing electronic devices with submicron dimensions. One advantage of this technique is that its resist exposure sensitivity is two or more orders of magnitude higher than that of e-beam lithography. Another advantage in submicron device fabrication is its negligible ion scattering in the resist and low back scattering from the substrate. Features as small as 6-8nm can be fabricated by using a 50kV $Ga^+$ two-lens microprobe system.

### 5.3.2 Etching

There are two kinds of FIB etching: physical sputter etching and chemical assisted etching using chemical reactions between the substrate surface and gas molecules adsorbed on the surface. Chemical assisted etching has several advantages over physical sputter etching: an increase in the etching rate, the absence of re-deposition, and little residual damage. The mechanisms of these etching processes are discussed in the references mentioned.

### 5.3.3 Deposition

There are two kinds of FIB deposition: chemical assisted deposition and direct deposition. Chemical assisted deposition uses chemical reactions between the

substrate surface and molecules adsorbed on the substrate. Direct deposition, on the other hand, uses low-energy (50eV) ions. FIB direct deposition has certain advantages over assisted deposition. A great advantage is that the purity of the deposited film is higher because of the high-vacuum conditions maintained during the deposition. FIB direct deposition promises to be useful for repairing devices such as integrated circuits and thin film transistors, and for repairing the clear defects in photo masks and x-ray masks.

### 5.3.4 Doping

FIB doping characteristics are nearly the same as those of conventional ion implantation. The throughput of FIB doping is lower than that of conventional ion implantation, so it is difficult to put this technique to practical use when making Si and GaAs devices. It can, however, be used to make quantum effects devices – at least in the research phase.

## 5.4 Usefulness of FIB system to this project

### 5.4.1 Requirements for the Capillary Hole

- Width of 1-2 microns for cell research and 3-4nm for DNA sequencing
- Uniform pore width
- Smooth pore walls to reduce noise
- The processes of lithography and etching can provide holes in the micron or even tenths of micron range only. FIB milling methods can easily drill holes in the nanometer range.

### 5.4.2 Advantages of using FIB to fabricate Nanopores

- The pores made from the FIB system can vary from microns to nanometers
- After drilling the hole, FIB deposition methods can be used to coat the inner surface with some desired ions to get smoother and more controlled pore dimensions.
- FIB can be used to sharpen, smoothen or etch some parts of the final structure after completion of the processing.
- High-aspect ratio trenches with almost parallel sidewalls can be milled by FIB.
- The only disadvantage of exposing a surface to FIB (either for etching, milling or microscopy) is that the constant bombardment with high-energy ions might damage the surface. So, some kind of sacrificial layer should be used to protect the layers underneath.

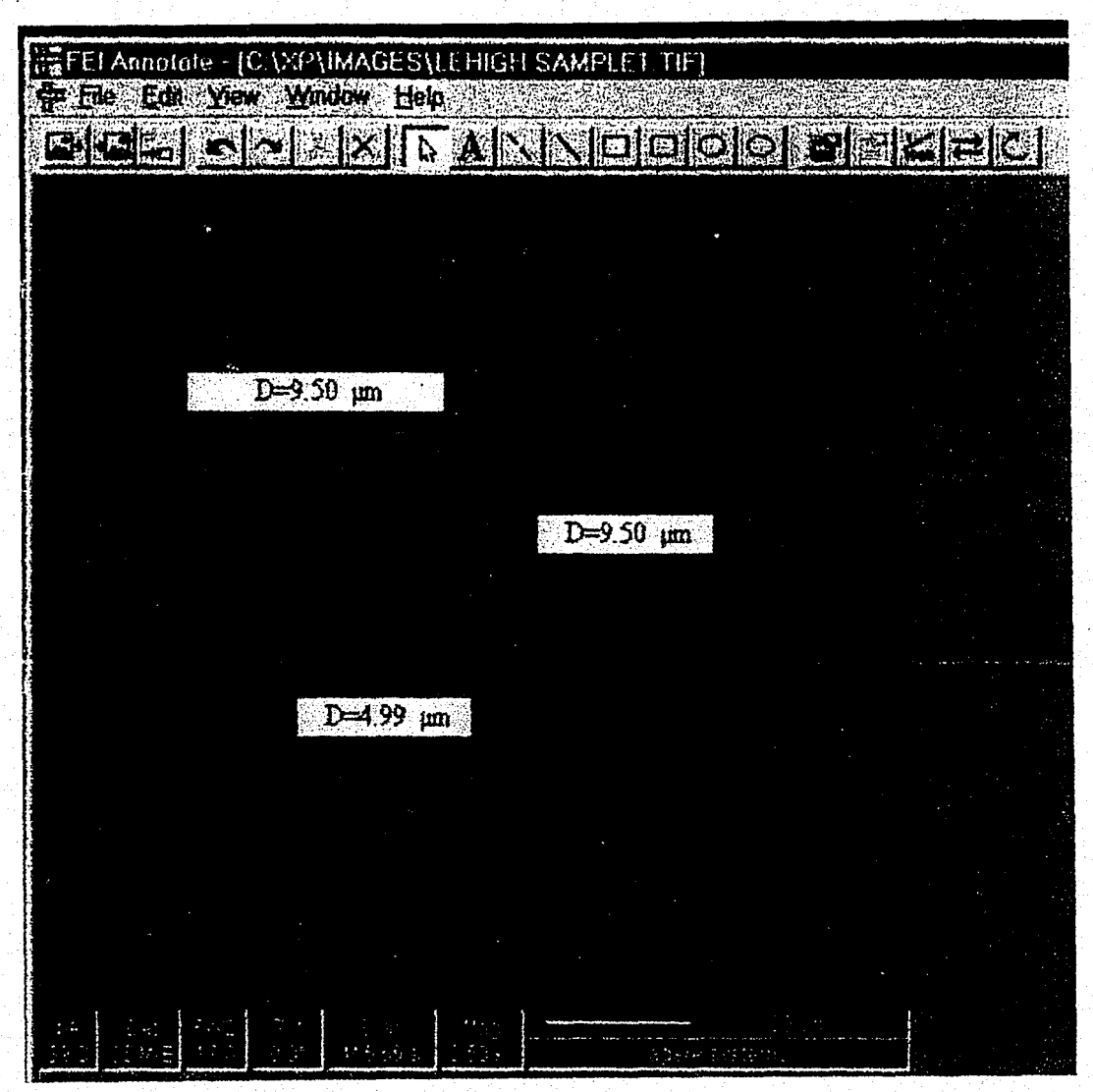


**Figure 5.3:** This figure shows the micropores drilled in the nitride membrane using the FIB system (my samples). The nitride membrane is around 800A° thick and is resting on a well (330µm deep) etched in silicon. It was possible to drill both square and circular holes of varying sizes in the nitride membrane using the FIB system.

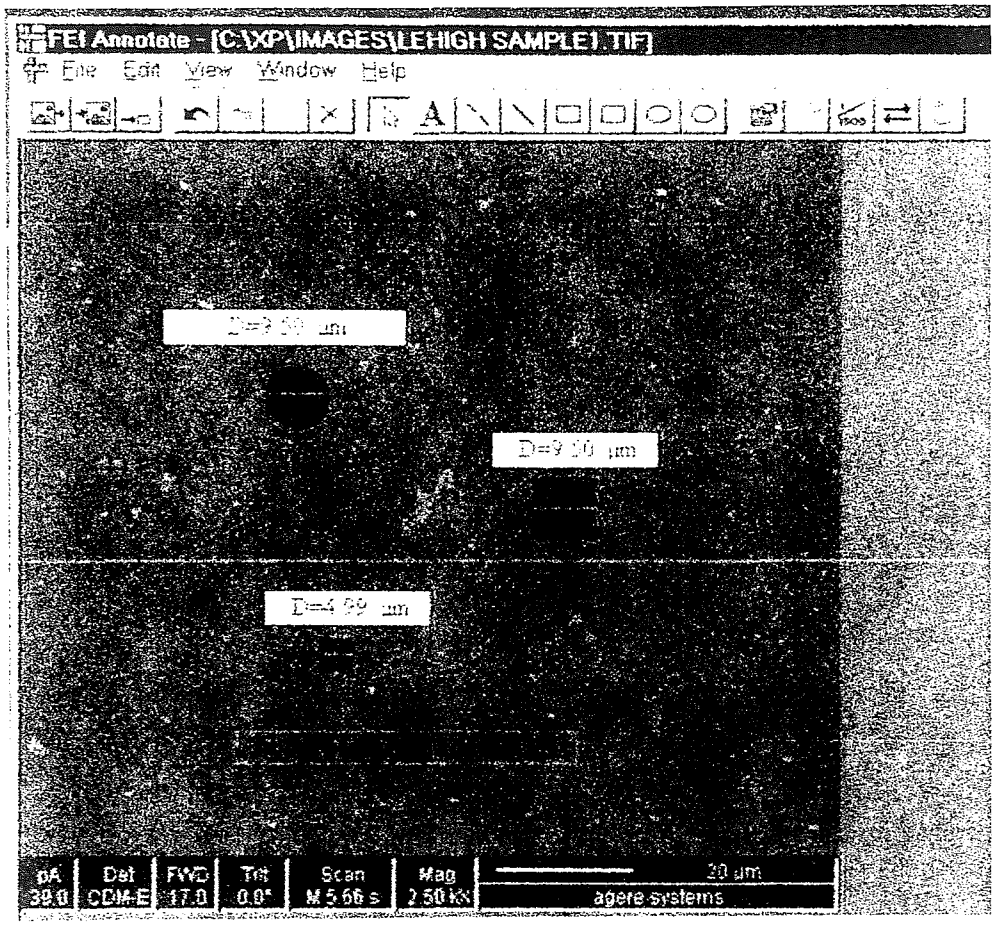


**Figure 5.3:** This figure shows the micropores drilled in the nitride membrane using the FIB system (my samples). The nitride membrane is around 800A° thick and is resting on a well (330µm deep) etched in silicon. It was possible to drill both square and circular holes of varying sizes in the nitride membrane using the FIB system.

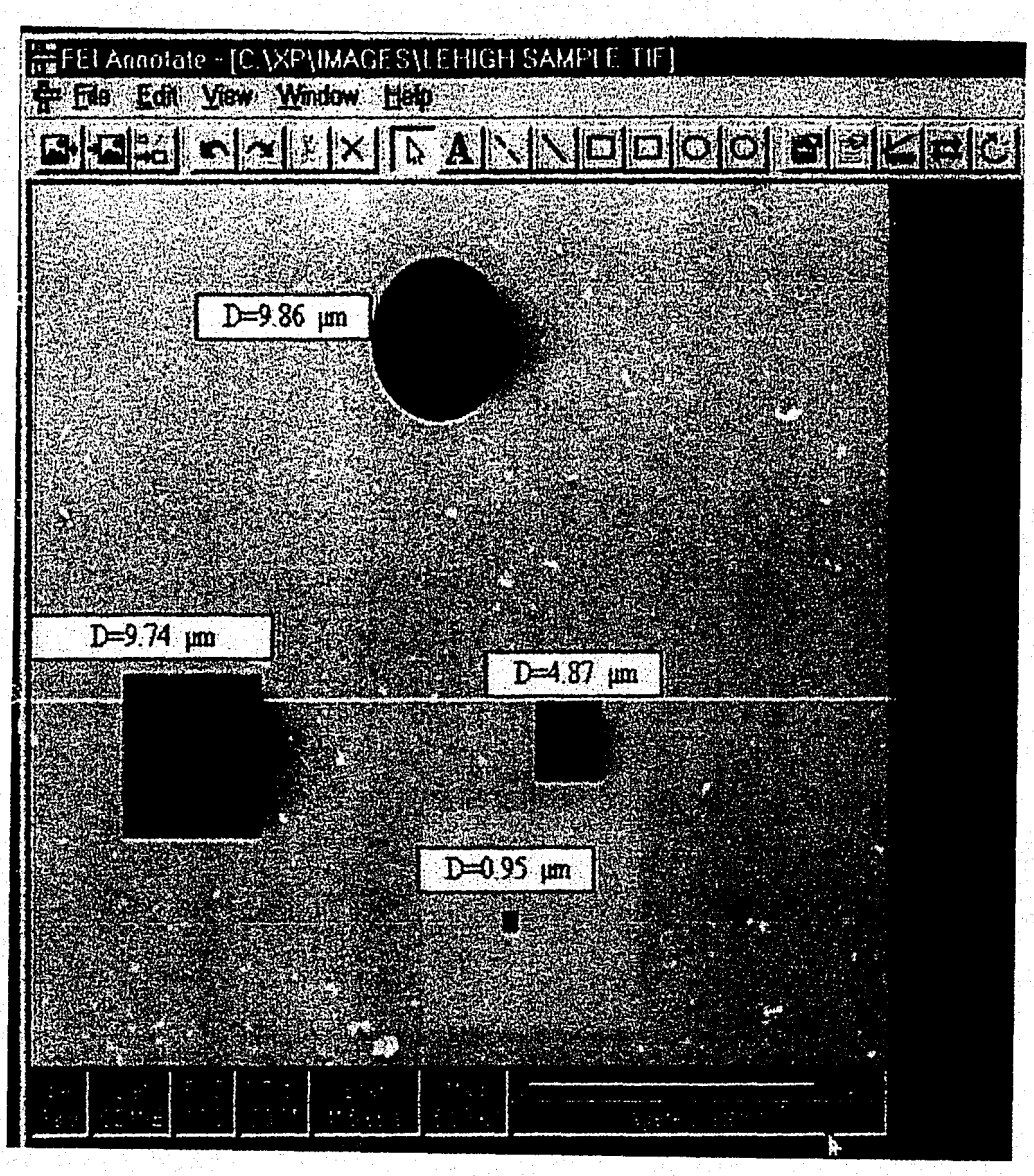


**Figure 5.4:** This figure shows some more holes drilled in the nitride membrane (my samples). The sizes of these holes are even smaller than the ones in Figure 6.3. Nanopores could also be drilled in a similar fashion but it's hard to see such small holes on a screen like the one above. However, AFM / SEM could be used to see such nanopores.

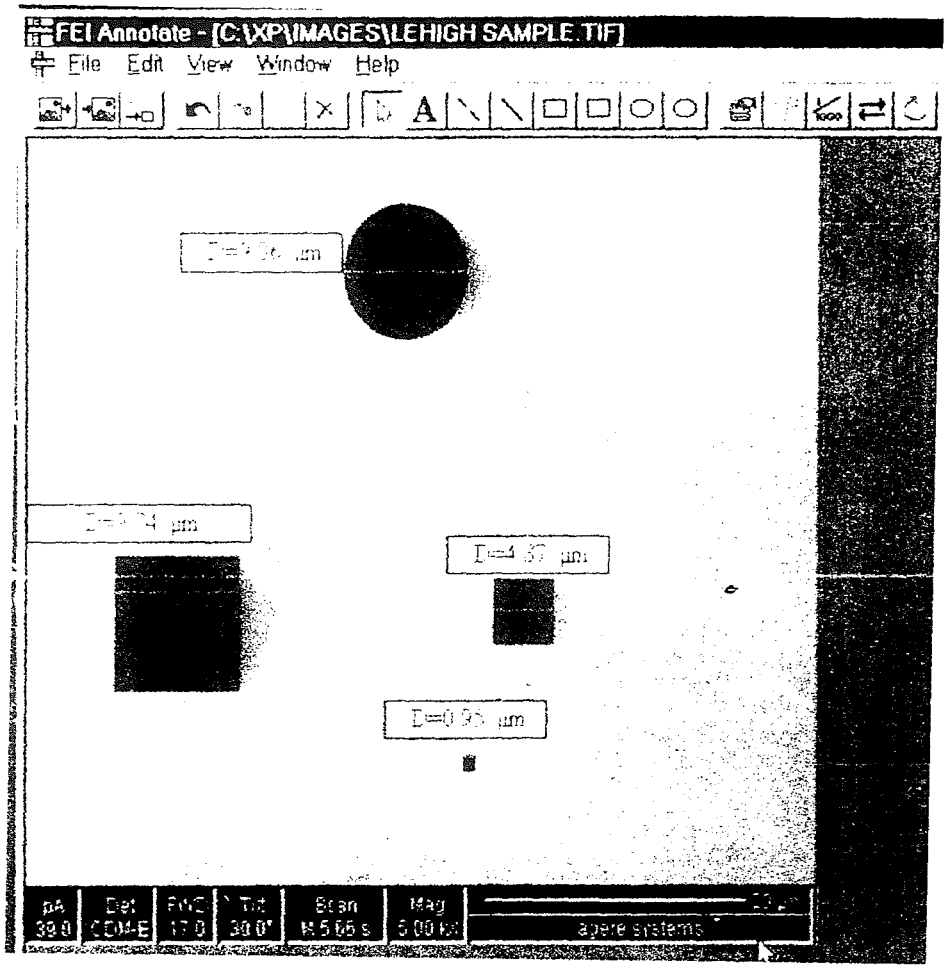


**Figure 5.4:** This figure shows some more holes drilled in the nitride membrane (my samples). The sizes of these holes are even smaller than the ones in Figure 6.3. Nanopores could also be drilled in a similar fashion but it's hard to see such small holes on a screen like the one above. However, AFM / SEM could be used to see such nanopores.

# Chapter 6
# Ultra-deep Silicon Etching in Aqueous KOH

## 6.1 Anisotropic Etching of Crystalline Silicon

Anisotropic etchants for crystalline silicon has been used for a long time. Their first applications included the etching of V-grooves on <100>silicon or U-grooves on <110>silicon, in order to fabricate MOS transistors for high power and high current densities [22,23]. Increasing attention has been paid to this etching technology, after recognizing its unique capabilities for micromachining three-dimensional structures. Due to the strong dependence of the etch rate on crystal direction and on dopant concentration, a large variety of silicon structures can be fabricated in a highly controllable and reproducible manner [24,25]. Typical structures include thin membranes, deep and narrow grooves, and cantilever beams with single or double sided suspensions [26-31].

All anisotropic etchants are aqueous alkaline solutions, where the main component can be either organic or inorganic [28]. Among the inorganic solutions, the one most frequently used is based on KOH. Several groups popularized the use of KOH as an anisotropic etchant for silicon [25,26]. They demonstrated unique ways of using the anisotropy of the etchant to fabricate mechanical structures in silicon. KOH etches the <100>surface of silicon at a rate about 400 times its etch rate on the <111>surface. Thus as etching proceeds, a square etch mask would create a pyramidal pit with sloped <111>sidewalls. These <111> faces intersect the wafer surface along the <110>directions and form an angle with the surface of $54.7^{\circ}$.

There are two limiting aspects of this process [22,23]. The first is that in order to create a hole with a depth equal to the thickness of the wafer, the upper opening must be at least 1.414 times the thickness of the wafer. One simple way to reduce the magnitude of this problem is to etch the wafer from both sides simultaneously. This double-sided process will reduce the minimum etch window by half. The second limitation is that in many applications it is essential that the sidewalls are vertical.

The etch rates of silicon by KOH not only depend on the crystal direction, the KOH concentration, the etching temperature, the doping concentration and the shape and alignment of the etchmask but also on the impurities in the etch chemicals, the illumination and probably the mechanical stress[24]. The latter particularly appears at the edges of the etchmask openings.

### 6.1.1 Etch rates of passivation layers

Passivation layers of particular interest are silicon dioxide and silicon nitride [24]. From measurements in the papers, the etch rate of LPCVD-Si nitride is less than 0.1 nm/h so for all practical applications it is regarded as a perfect masking material. In contrast to silicon nitride, silicon dioxide shows a finite etch rate for any etchant used. The etch rate of a thermal oxide grown at 1000° C is approximately 30% lower than the etch rate of a CVD oxide deposited at 800° C. When the $SiO_2$ etch rate is plotted as a function of the KOH concentration, it exhibits a maximum at approximately 35% [22,25,26]. Below this concentration, a linear increase of the etch rate with the KOH concentration is observed. At higher concentrations, the decrease corresponds roughly to the square of the molar water concentration. The etch rate

ratios between silicon and $SiO_2$ are very important for practical applications when the oxide is used as a masking layer during etching. The ratio depends strongly on the composition of the etchant and the temperature. In applications where the full thickness of the wafer is to be etched off, a KOH solution with a concentration of about 20% at a lower temperature is recommended [22]. Then the attainable ratio is on the order of about 1000, which is satisfactory.

- In order to mask silicon wafers, thermal oxide and/or LPCVD silicon nitride layers are commonly used. The etch rate of LPCVD-Si nitride in KOH is close to zero. As a result of the different thermal expansion coefficients of the masking layer and the silicon substrate, the coated silicon wafer suffer from residual film stress [24]. In the case of an LPCVD-Si nitride etchmask, the intrinsic stress must be considered as the primary source of the mechanical stress. Continuous films produce only low stresses in the silicon substrate but discontinuities, like masking openings, introducing large localized stress fields. Studies done on the mechanical stress in LPCVD-Si nitride etchmask openings suggest the following [24]:
- Due to the high tensile stress in the LPCVD-Si nitride etchmask, high local mechanical stress fields appear in the silicon substrate along the etchmask edge. The highest values are reached at convex corners.
- The thicker the nitride etchmask, the higher is the stress in the substrate.

It has been observed that convex corners with thick LPCVD-Si nitride always show notches on their facets. For the lower thickness these have never been observed. These notches are caused by cracks in the highly stressed

LPCVD-Si nitride layer during corner undercutting. As $SiO_2$ films show compressive stress, an intermediate $SiO_2$ film can be used to compensate for the high tensile stress of the LPCVD-Si nitride etchmask. However, there is a higher lateral underetching and curved etch edges at chips with double-layer $SiO_2/Si_3N_4$ etch-masks compared with the single layer LPCVD-Si nitride etchmasks. Thus, the $SiO_2$ layer leads to a lower anisotropy ratio [24].

In this project, the final desired structure is to have a micro/nanopore in a thin membrane, which is resting on the silicon substrate. To achieve this, the silicon substrate had to be etched completely to have the wells on which the Si nitride membrane can be resting. Because of the stress considerations in a single layer of Si-nitride (as mentioned above), it was advisable to use $SiO_2$ / $Si_3N_4$ etch-masks instead of a single layer of Si-nitride on the silicon substrate. Also, because the thickness of the membrane (in my case) is not so big (<900A°), there were not any cracks or notches in the membrane. The smoothness of the sidewalls of the wells formed after etching depends on the purity of the KOH solution and the temperature [27]. As will be shown shortly, the surfaces formed by using the same solution over and over again are not so smooth and they have residues (probably oxide or silicon) sitting at the bottom. If a fresh solution is used for the etching process each time, the wells look neat and clean. Also, lower temperature of operation and a lower concentration of the KOH solution give better results. During my etching experiments, I tried three different concentrations of solutions (12%, 20%, 40%) and three different temperature conditions (60°C, 80°C, 95°C). The best results were obtained using 20% KOH solutions at 80°C. At the temperature of 60°C, the etching process is slow and

there is not a marked difference in the quality of the wells as compared to at the temperature of 80°C. A higher concentration of the KOH solution speeds up the etching process but gives more roughness on the surfaces of the wells [31].

Constant stirring the wafers in the KOH bath solution helps in the improving the quality of the surfaces of the wells. The position the wafers are kept sitting in the bath solution affects the quality of the wells as well. We know that when silicon is etched in KOH, hydrogen is formed which tries to escape the solution in the form of gas bubbles. My wafers were double-sided polished and a Si-nitride mask protected the backside. The front side of the wafer was placed facing up so that the hydrogen bubbles formed during the silicon etching could escape the KOH solution with ease. If the hydrogen bubbles were not given that ease to escape, they would get 'stuck' inside the well for a while, leading to pit holes and additional roughness in the inside surface of the well [27,31]. In my wafers I never encountered such pit holes because of the correct manner of placing of my wafers in the KOH solution.

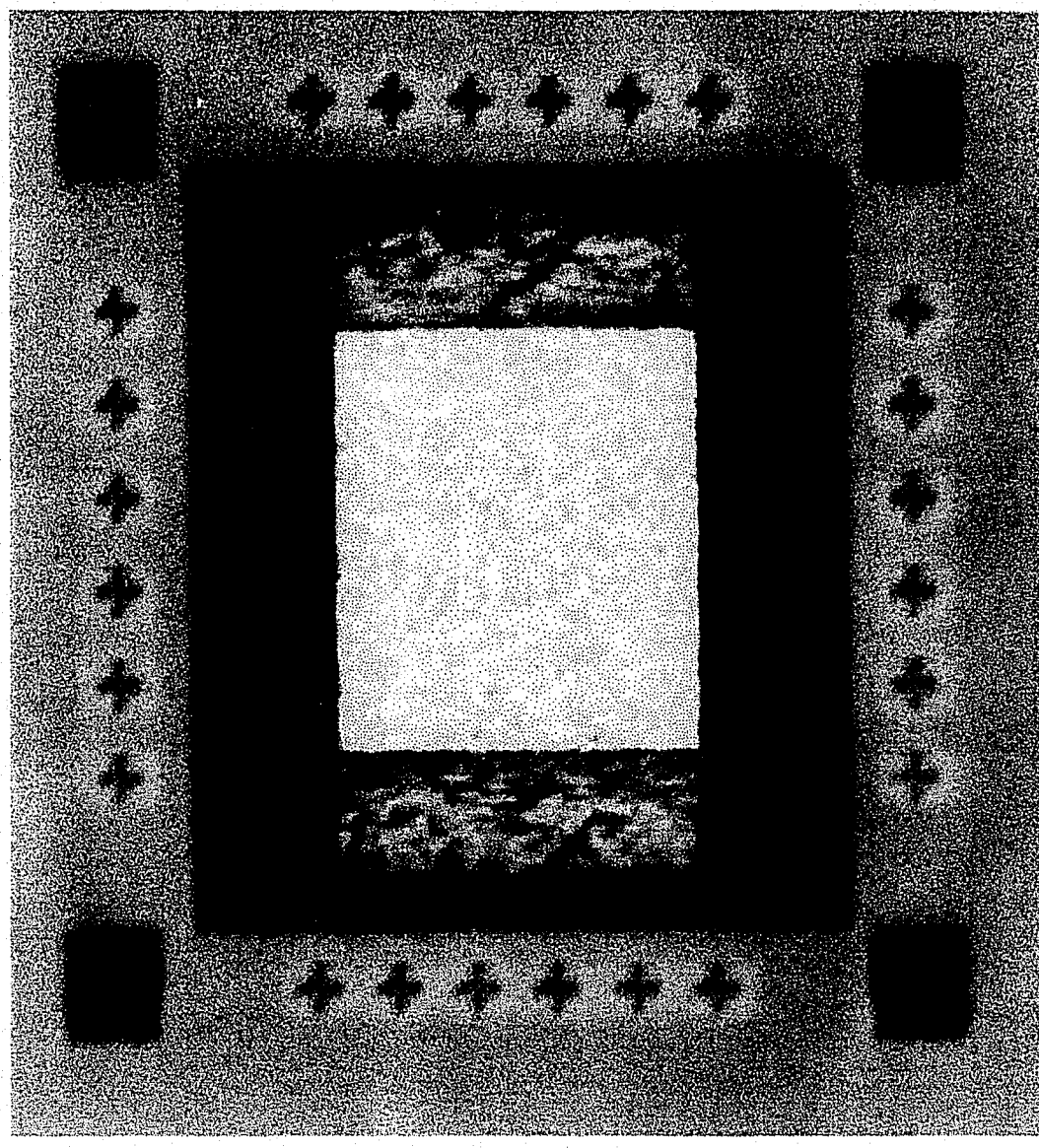

**Figure 6.1:** This picture shows a 330μm pyramidal well etched in a 330μm thick silicon wafer. The inner surfaces of this well look clean without much deposits/residues, cracks or notches. It took around 6 hours to etch this well in a 20% KOH solution. The inside of the well exposes the oxide, which is on the other side of the wafer. The picture was taken before the final BHF dip to remove the front oxide.

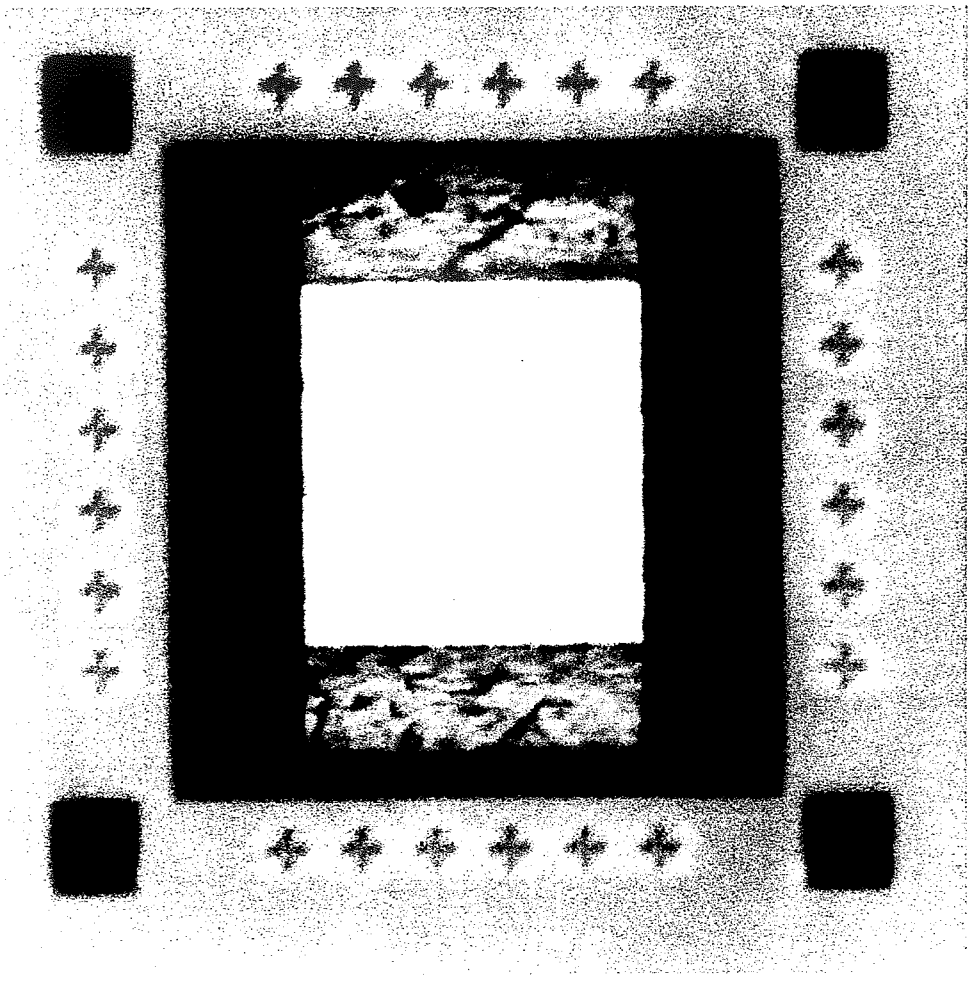

**Figure 6.1:** This picture shows a 330μm pyramidal well etched in a 330μm thick silicon wafer. The inner surfaces of this well look clean without much deposits/residues, cracks or notches. It took around 6 hours to etch this well in a 20% KOH solution. The inside of the well exposes the oxide, which is on the other side of the wafer. The picture was taken before the final BHF dip to remove the front oxide.

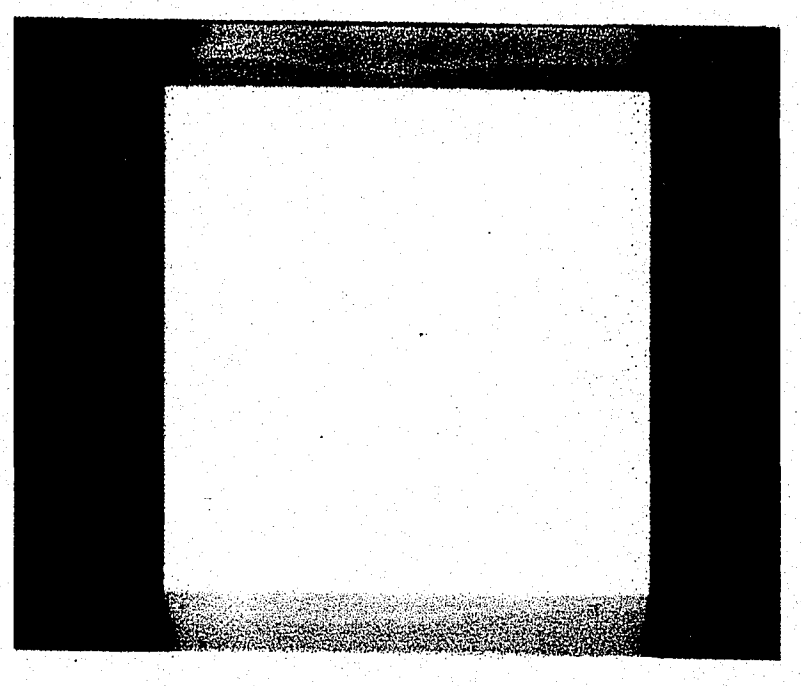

**Figure 6.2:** This picture was taken after the final BHF dip was completed. The remaining oxide residues are all dissolved and the inside surface looks neat and clean. The nitride on the other side is exposed and appears to be transparent in light. The etching was performed at 85°C with 20% fresh KOH solution.

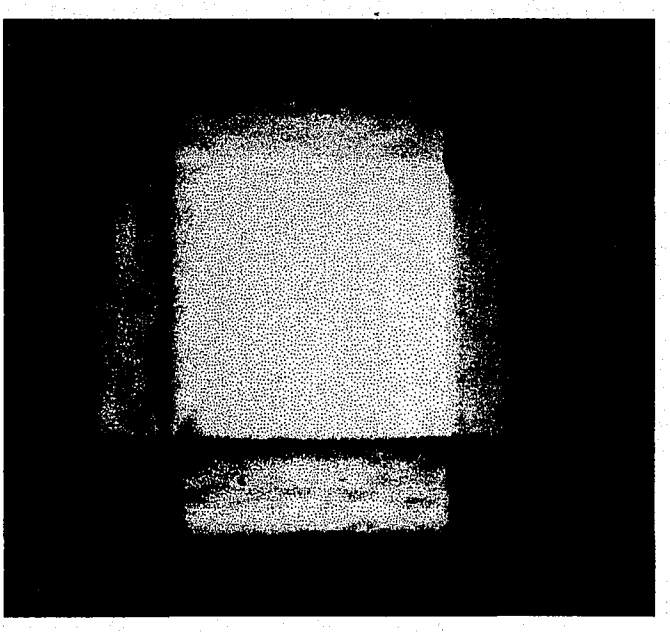

**Figure 6.3:** This picture shows yet another well etched in silicon. The etching was performed at 95°C and with a used KOH solution (20%). The smoothness of the sidewalls is pretty good but not as the one in Figure 6.2.

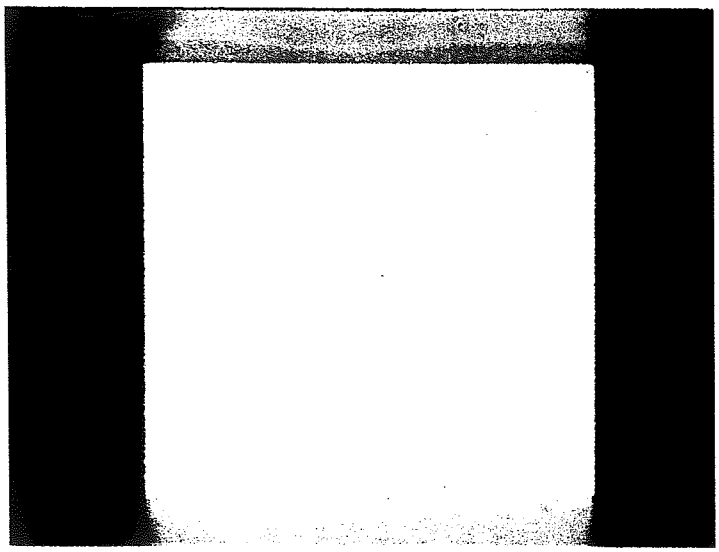

**Figure 6.2:** This picture was taken after the final BHF dip was completed. The remaining oxide residues are all dissolved and the inside surface looks neat and clean. The nitride on the other side is exposed and appears to be transparent in light. The etching was performed at 85°C with 20% fresh KOH solution.

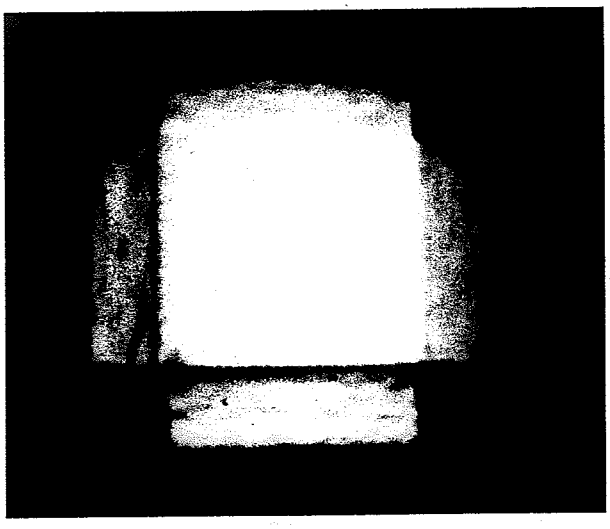

**Figure 6.3:** This picture shows yet another well etched in silicon. The etching was performed at 95°C and with a used KOH solution (20%). The smoothness of the sidewalls is pretty good but not as the one in Figure 6.2.

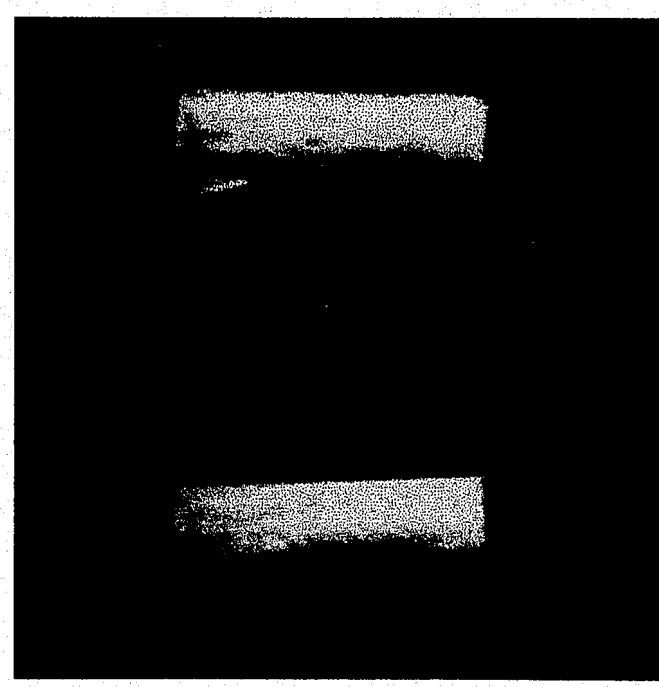

**Figure 6.4:** This picture shows well etched in silicon with a ruptured nitride membrane. The nitride membrane collapsed in this case because of over-etching which the thin membrane could not withhold.

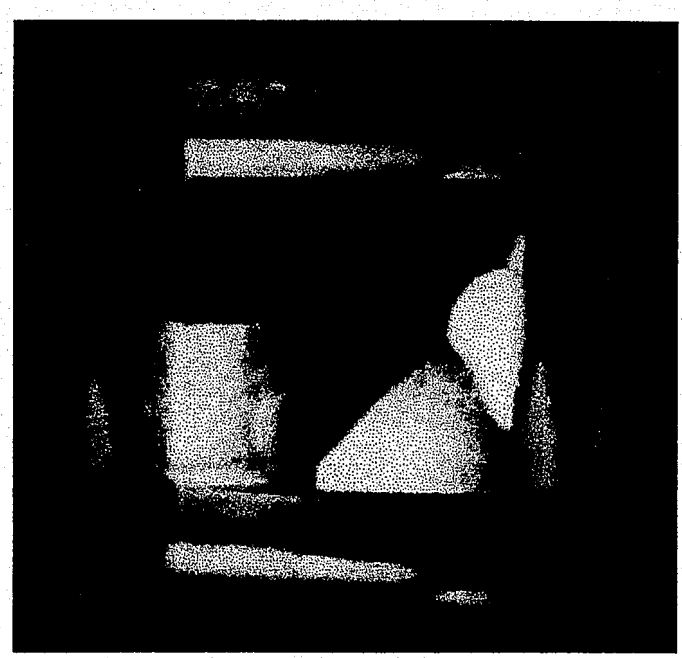

**Figure 6.5:** This picture shows a well in silicon with a nitride membrane that has ruptured but is still hanging from the sidewalls. The reason for the membrane rupture is over-etching too.

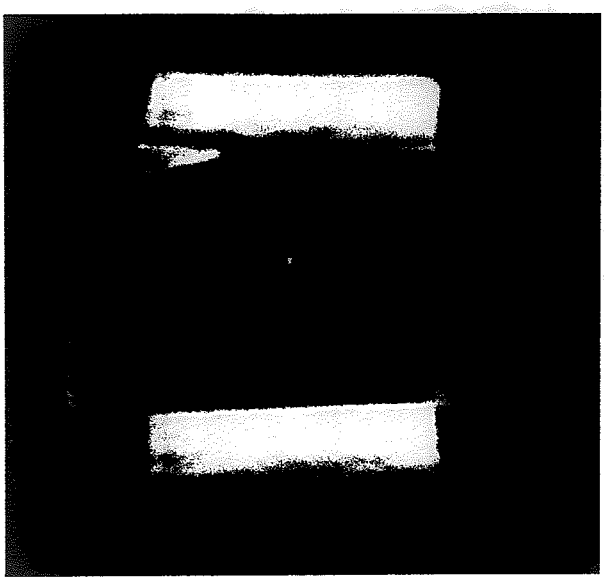

**Figure 6.4:** This picture shows well etched in silicon with a ruptured nitride membrane. The nitride membrane collapsed in this case because of over-etching which the thin membrane could not withhold.

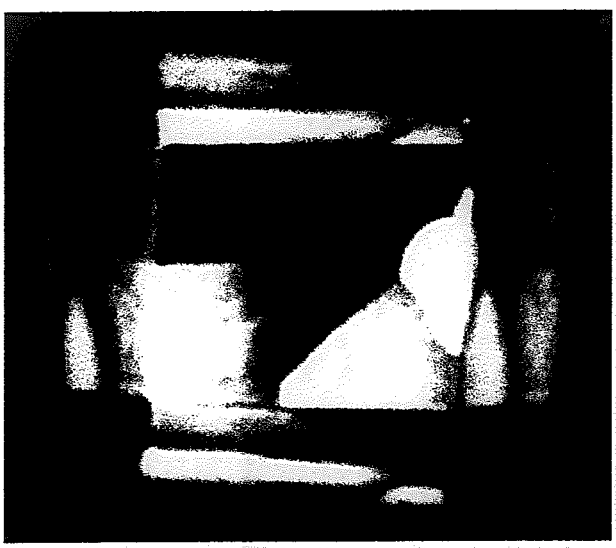

**Figure 6.5:** This picture shows a well in silicon with a nitride membrane that has ruptured but is still hanging from the sidewalls. The reason for the membrane rupture is over-etching too.

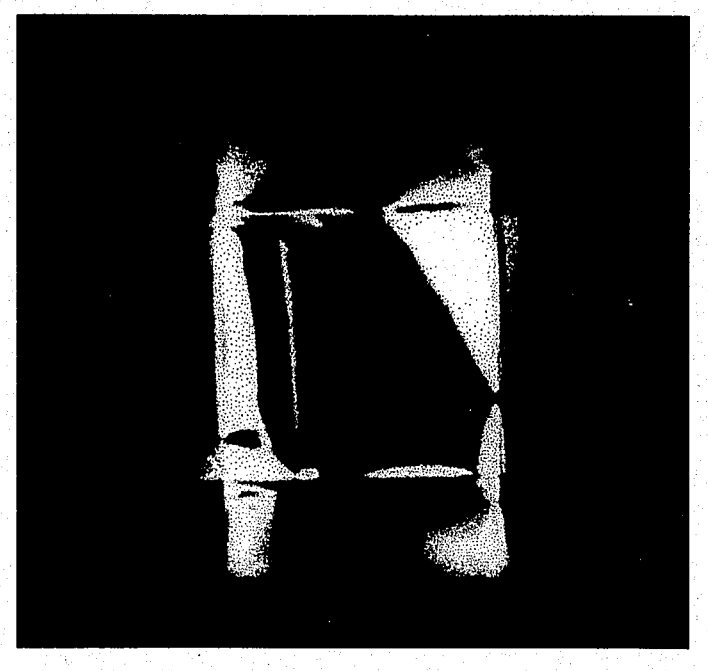

**Figure 6.6:** This picture shows a well etched in silicon with a rupture nitride membrane. In this case, the membrane collapsed during the process of drilling holes using the FIB system. On an average, one out of five nitride membranes collapsed while drilling micro/nanopores in them.

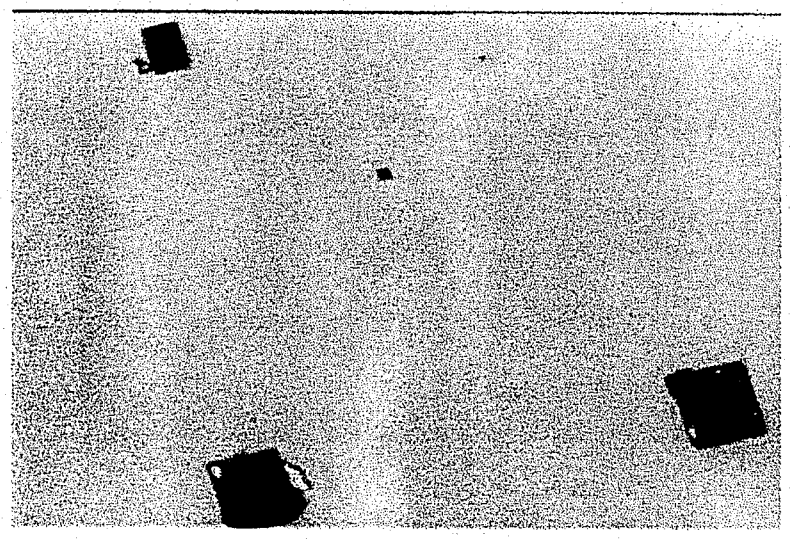

**Figure 6.7:** This picture shows the front side of the wafers after the process of silicon etching is over. Some parts of the wafer show openings like the one shown above when the wafer is over-etched. But when the etching is timed and monitored constantly, such openings or holes do not occur.

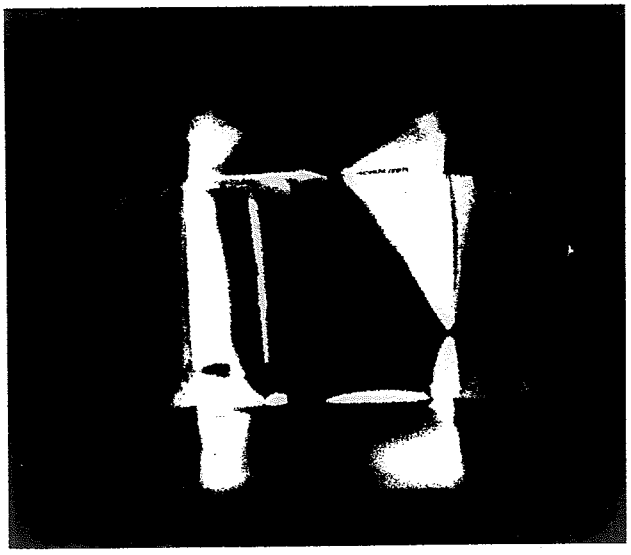

**Figure 6.6:** This picture shows a well etched in silicon with a rupture nitride membrane. In this case, the membrane collapsed during the process of drilling holes using the FIB system. On an average, one out of five nitride membranes collapsed while drilling micro nanopores in them.

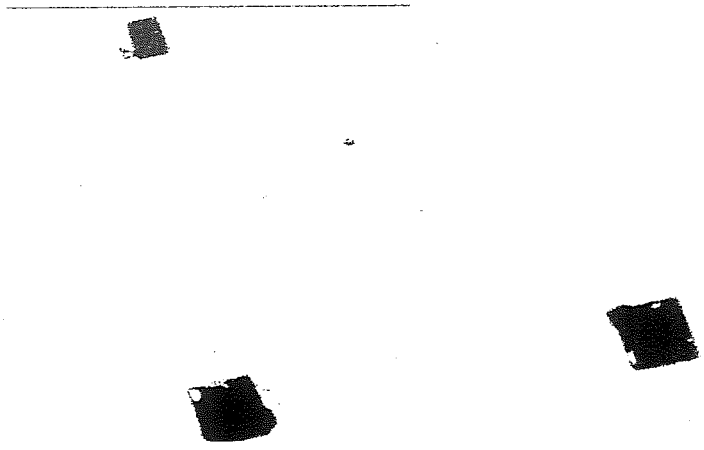

**Figure 6.7:** This picture shows the front side of the wafers after the process of silicon etching is over. Some parts of the wafer show openings like the one shown above when the wafer is over-etched. But when the etching is timed and monitored constantly, such openings or holes do not occur.

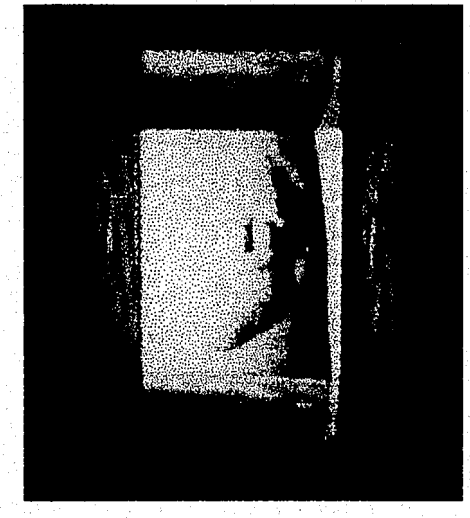

Figure 6.8

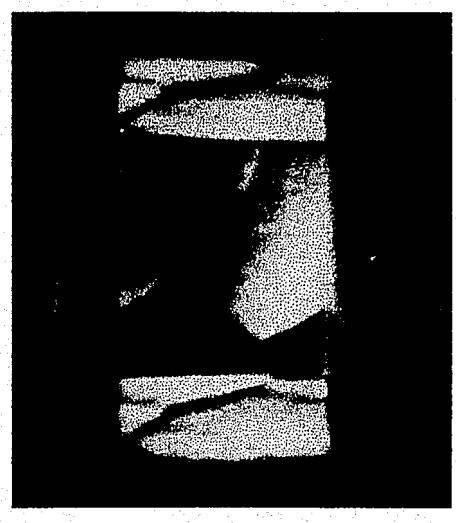

Figure 6.9

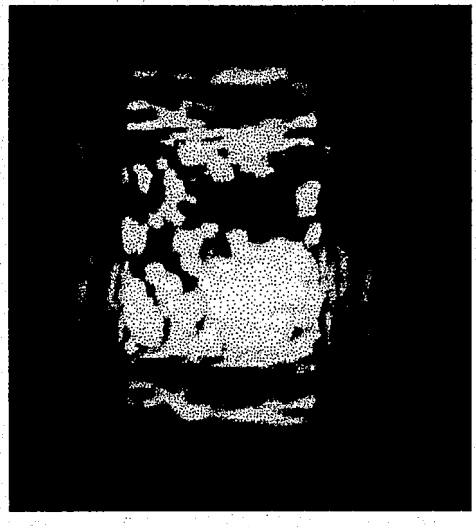

Figure 6.10

**Figures 6.8, Figure 6.9** and **Figure 6.10** show the different forms/shapes and sizes of deposits and residues that can accumulate inside the well during and after the process of silicon etching.

**Figure 6.8** shows the silicon residues and deposits collected inside the well when the etching is not complete and the oxide/nitride membrane has not been reached.

**Figure 6.9** shows the inside surface of the well just 0.5-1 hour before the completion of the etching process. The residues and deposits here are also the etched silicon.

**Figure 6.10** shows the well after the etching process is completed. The residues and deposits are from the oxide, which is now being attacked by the KOH. After BHF dip these residues are no longer seen.

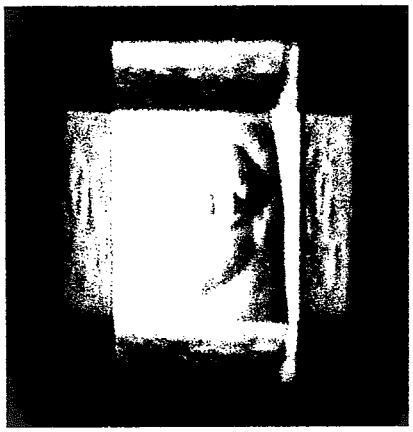

Figure 6.8

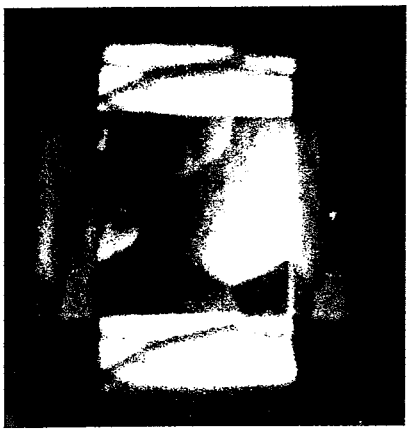

Figure 6.9

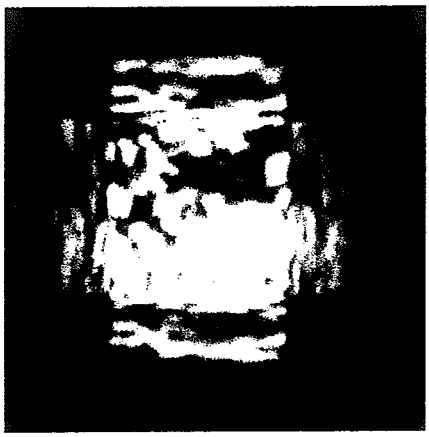

Figure 6.10

**Figures 6.8. Figure 6.9** and **Figure 6.10** show the different forms/shapes and sizes of deposits and residues that can accumulate inside the well during and after the process of silicon etching.

**Figure 6.8** shows the silicon residues and deposits collected inside the well when the etching is not complete and the oxide/nitride membrane has not been reached.

**Figure 6.9** shows the inside surface of the well just 0.5-1 hour before the completion of the etching process. The residues and deposits here are also the etched silicon.

**Figure 6.10** shows the well after the etching process is completed. The residues and deposits are from the oxide, which is now being attacked by the KOH. After BHF dip these residues are no longer seen.

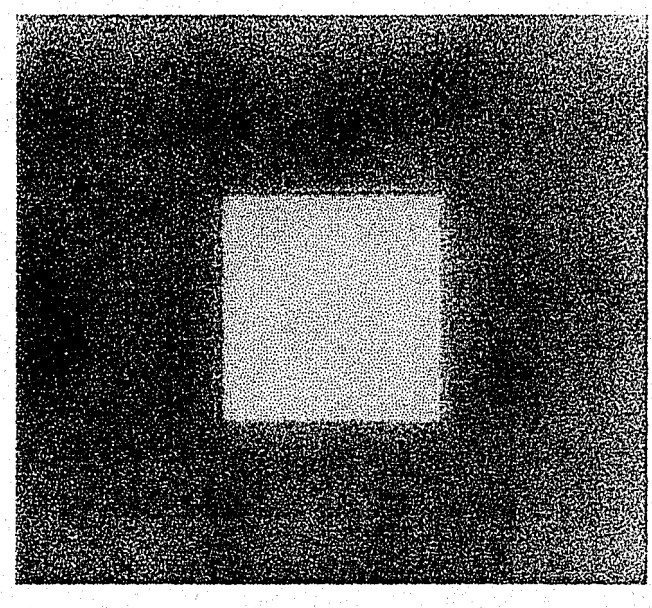

**Figure 6.11:** This picture shows the front side of the wafer, which has the nitride membrane resting on a 330μm deep well. The nitride appears to be transparent to light when seen under the optical microscope.

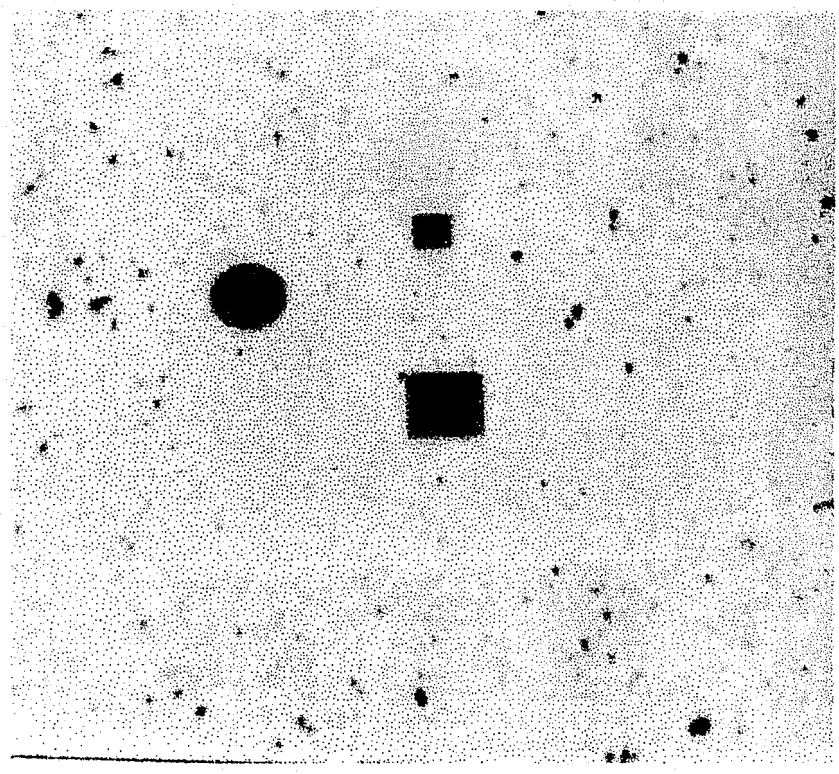

**Figure 6.12:** This picture shows the micropores drilled in the nitride membrane using the FIB system (my samples).

For the sake of comparison, I tried to etch micropores in an oxide/nitride layer using photolithography. The silicon oxide was around 1000A° thick and the silicon nitride layer above it was around 500A° thick. The nitride was etched using Plasma Etching for around 40 seconds. The pictures from the AFM reveal the resulting nature of the surface after etching is complete. The limitation of the etching technique to make holes becomes evident in the submicrometer and nanometer dimensions when the only answer to our questions is the FIB system.

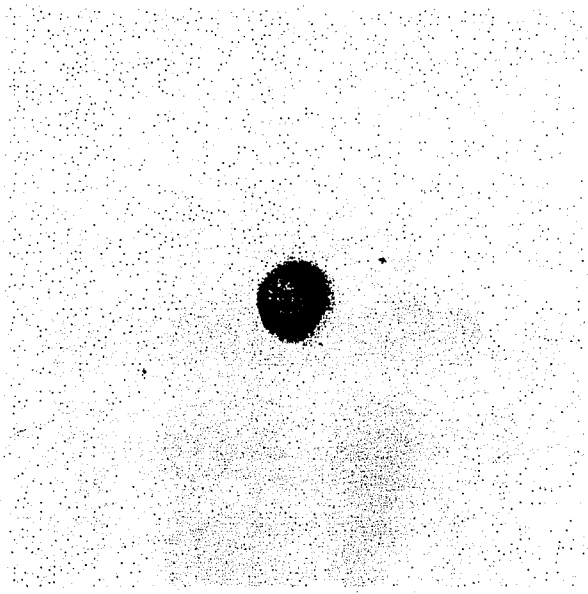

**Figure 6.13:** This picture shows a 4μm diameter circular hole etched in the nitride/oxide layer.

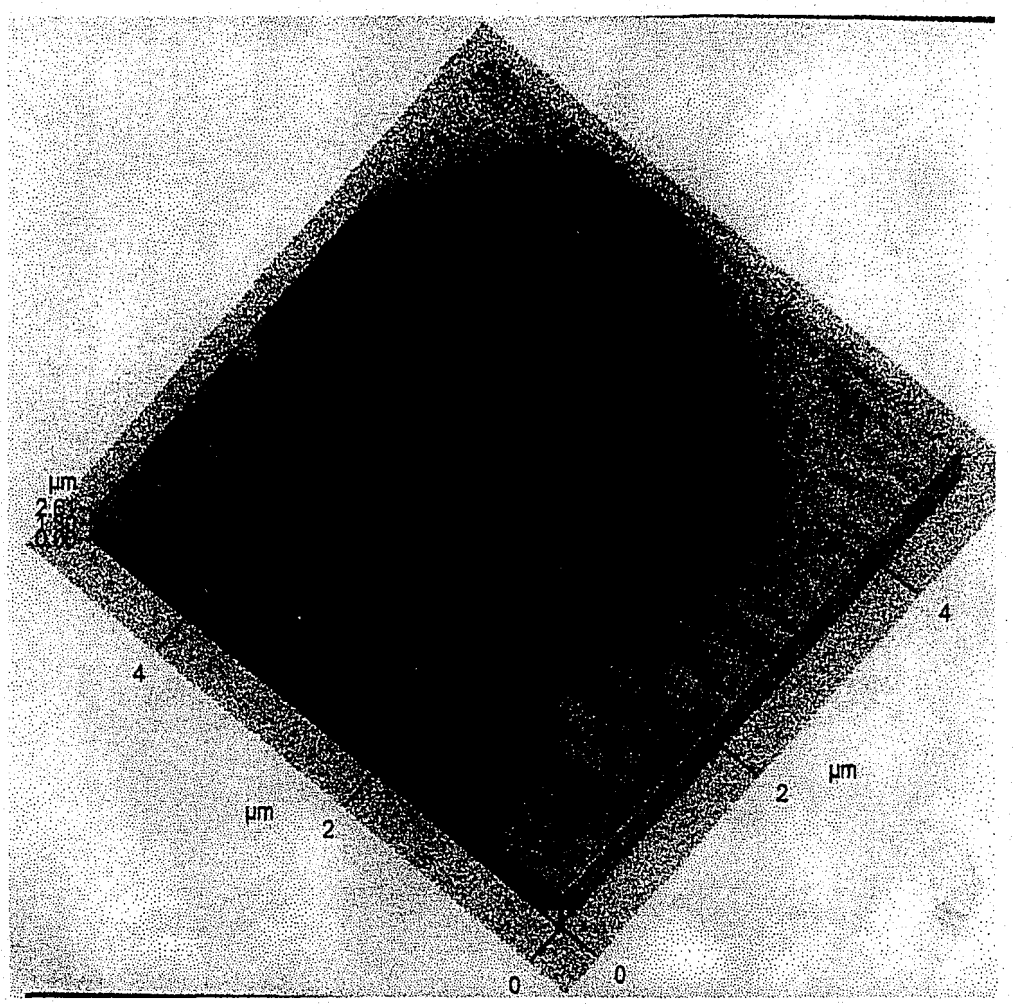


**Figure 6.14:** This picture is taken from the AFM and shows the 4µm hole chemically etched in the oxide/nitride layer. The hole is actually not that deep (around 1200A°) which is why the perception of the hole is not so distinct.

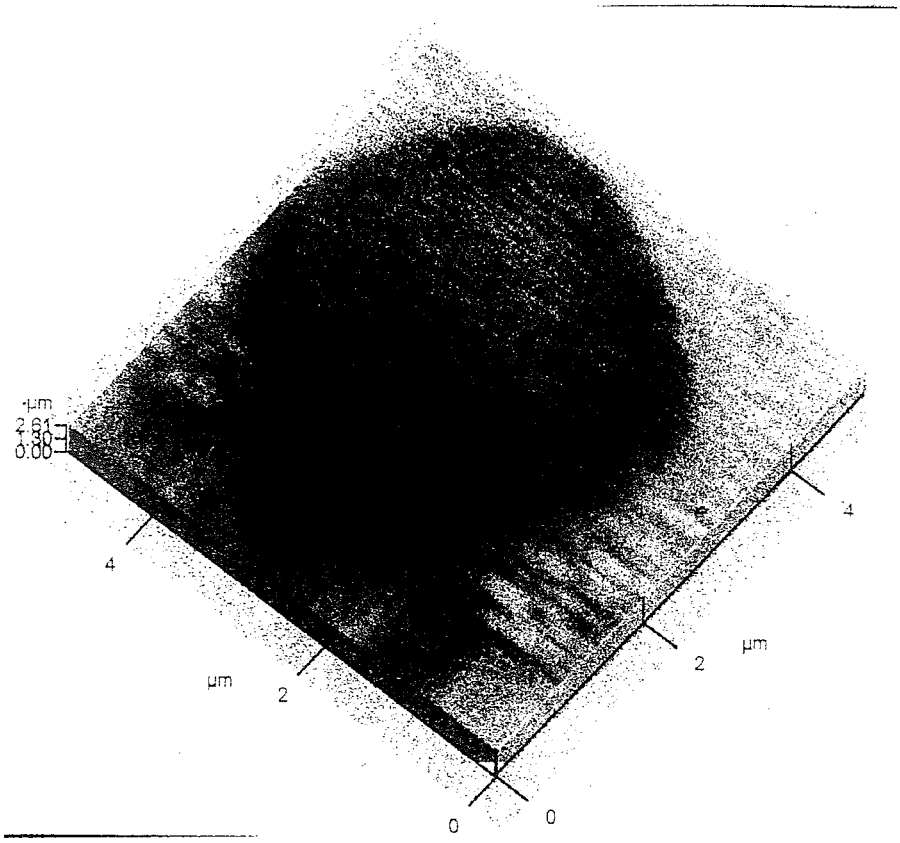


**Figure 6.14:** This picture is taken from the AFM and shows the 4µm hole chemically etched in the oxide nitride layer. The hole is actually not that deep (around 1200A°) which is why the perception of the hole is not so distinct.

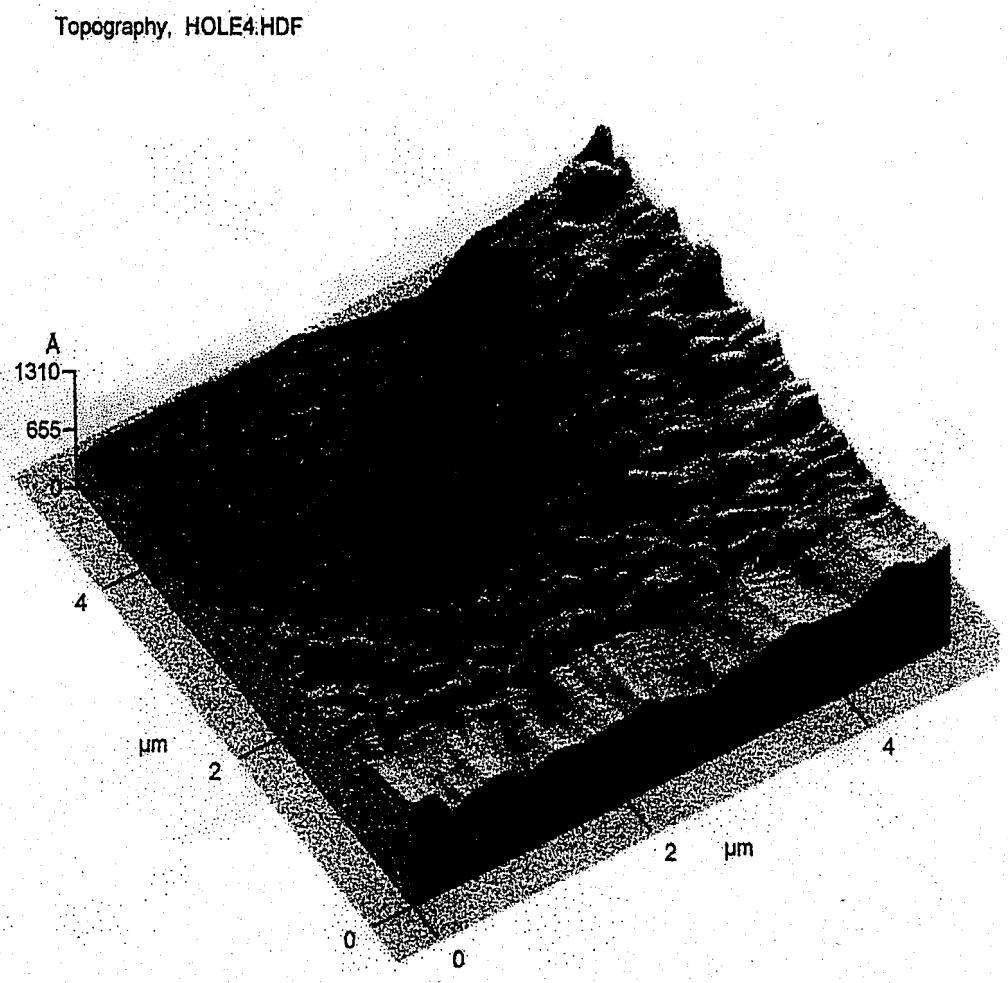


**Figure 6.15:** This AFM picture shows the texture of the surfaces after the hole was chemically etched in silicon. It can be seen that plasma etching (of the nitride) increases the surface roughness and chemical etching (of the oxide) after that still adds to the roughness.

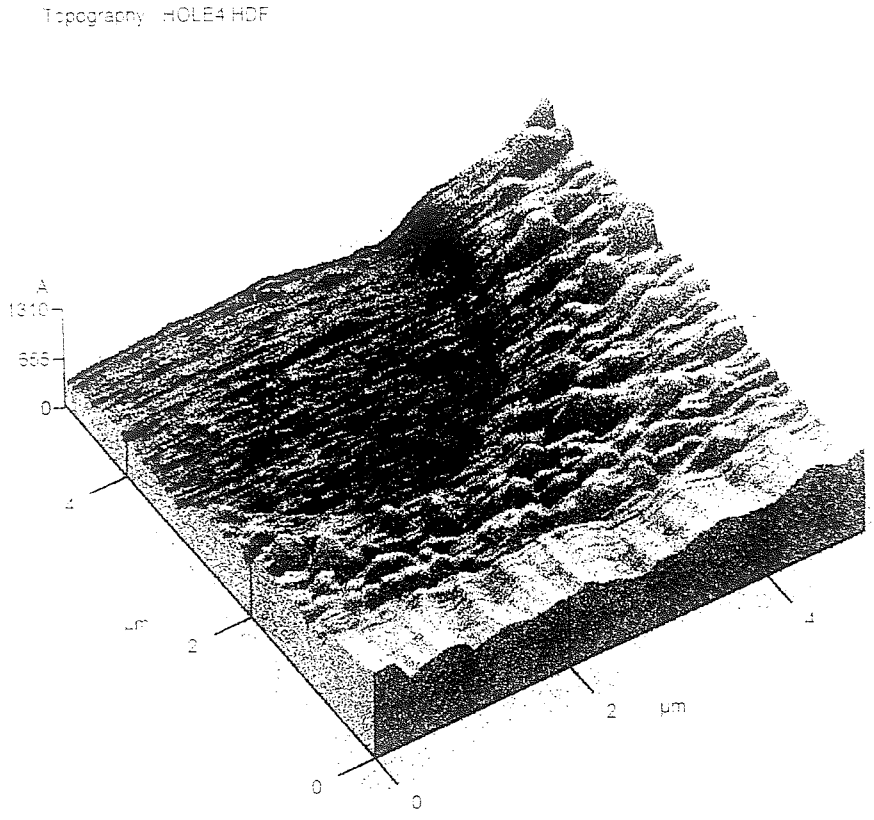


Figure 6.15: This AFM picture shows the texture of the surfaces after the hole was chemically etched in silicon. It can be seen that plasma etching (of the nitride) increases the surface roughness and chemical etching (of the oxide) after that still adds to the roughness.

# Conclusion

In this work, we have discussed the different techniques used to fabricate a micro/nanopore in a thin membrane resting on silicon well. This structure can be visualized as a planar micropipette used for the measurement of single-channel ionic currents. The work in this thesis is the first step towards building a Biochip for cellular measurements. The processing steps discussed in this thesis work good and the results are encouraging too. It should now be possible to design all the masks needed and fabricate the final structure in its entirety. Also, the task of circuit design and simulation is to be done, after which it would be possible to lay the circuit on-chip along with the micro/nanopores.

# References:


[1] Thomas Weiss, "Cellular Biophysics – Electrical Properties", *MIT Press,* 1996 Edition, Volume 2.

[2] Bert Sakmann and Erwin Neher, " Single-Channel Recording", *Plenum Press, New York,* Second Edition.

[3] R.A. Levis and J.L. Rae, "Constructing a Patch-Clamp Setup", *Methods in Enzymology,* Volume 207, page 18-66.

[4] O.P. Hamill et. al., "Improved patch-clamp techniques for high resolution current recording from cells and cell-free membrane patches", *Pflugers Archiv,* Volume 391, page 85-100.

[5] F.J. Sigworth, "Design of the EPC-9, a computer-controlled patch clamp amplifier. 1. Hardware", *Journal of Neuroscience Methods,* Volume 56, page 88-107.

[6] F.J. Sigworth, "Design of the EPC-9, a computer-controlled patch clamp amplifier. 2. Software", *Journal of Neuroscience Methods,* Volume 56, page 108-118.

[7] David Lubensky and David Nelson, "Driven Polymer Translocation Through a Narrow Pore", *Biophysical Journal,* Volume 77, page 1824-1838 (October 1999).

[8] Amit Meller et. al., "Rapid nanopore discrimination between single polynucleotide molecules", *PNAS,* Volume 97, page 1079-1084 (February 2000).

[9] Basil Hanss et. al., "Identification and characterization of a cell membrane nucleic acid channel", *PNAS,* Volume 95, page 1921-1926 (February 1998).

[10] Mark Akeson et. al., "Microsecond Time-Scale Discrimination Among Polycytidylic Acid, Polyadenylic Acid and Polyuridylic Acid as Homopolymers or as Segments within Single RNA Molecules", *Biophysical Journal,* Volume 77, page 3227-3233 (December 1999).

[11] Denis Wirtz, "Direct Measurement of the Transport Properties of a Single DNA Molecule", *Physical Review Letters,* Volume 75, No. 12, page 2436-2439 (September 1995).

[12] Marvin White, "A BioChip for Ion Channel Research and Electronic DNA Sequencing", *NSF Proposal,* June 2000.

[13] H.S. Wong and Marvin White, "A CMOS Integrated ISFET Operational Amplifier Chemical Sensor employing Differential Sensing", *IEEE Transactions on Electron Devices,* Volume 36, page 3-6, March 1989.

[14] Kenji Gamo, "Recent Advances of focused ion beam technology", *Nuclear Instruments and Methods in Physics Research B,* Volume 121, page 464-469 (1997).

[15] Kenji Gamo, "Focused Ion Beam Technology", *Vacuum,* Volume 42, page 89-98 (1991).

[16] Shinji Matsui and Yukinori Ochiai, "Focused ion beam applications to solid state devices", *Nanotechnology,* Volume 7, page 247-258 (1996).

[17] J. Brugger et. al., "Silicon Micro/Nanomechanical Device Fabrication Based on Focused Ion Beam Surface Modification and KOH Etching", *Microelectronic Engg,* Volume 35, page 401-404 (1997).

[18] U. Dotsch and A.D. Wieck, "Nanodevices produced with focused ion beams", *Nuclear Instruments and Methods in Physics Research B,* Volume 139, page 12-19 (1998).

[19] R.L. Kubena et. al., " A low magnification focused ion beam system with 8nm spot size", *Journal of Vacuum Science and Technology B,* Volume 9(6), Nov/Dec 1991.

[20] M.J. Vasile et. al., "Microfabrication techniques using focused ion beams and emergent applications", *Micron,* Volume 30, page 235-244 (1999).

[21] John Melngalis, "Focused ion beam technology and applications", *Journal of Vacuum Science and Technology B,* Volume 5(2), March/April 1987.

[22] H. Seidel et. al., "Anisotropic Etching of Crystalline Silicon in Alkaline Solutions, 1. Orientation Dependence and behavior of Passivation Layers", *Journal of Electrochemical Society,* Volume 137, No. 11, page 3612-3625.

[23] H. Seidel et. al., "Anisotropic Etching of Crystalline Silicon in Alkaline Solutions, 2. Influence of Dopants", *Journal of Electrochemical Society,* Volume 137, No. 11, page 3626-3632.

[24] H. Schroder et. al., "Effects of the etchmask properties on the anisotropy ratio in the anisotropic etching of 100 silicon in aqueous KOH", *Journal of*

*Micromechanics and Microengg"*, Volume 8, page 99-103 (1998).

[25] Irena Barycka and Irena Zubel, "Silicon anisotropic etching in KOH-isopropanol etchant", *Sensors and Actuators A,* Volume 48, page 229-238 (1995).

[26] E. van Veenendaal et. al., "Simulation of anisotropic wet chemical etching using a physical model", *Sensors and Actuators A,* Volume 84, page 324-329 (2000).

[27] Irena Zubel, "Silicon anisotropic etching in alkaline solutions. 2.On the influence of anisotropy on the smoothness of etched surfaces", *Sensors and Actuators A,* Volume 70, page 260-268 (1998).

[28] Kirt Williams and Richard Muller, "Etch Rates for Micromachining Processing", *Journal of Microelectromechanical Systems,* Volume 5, No. 4, page 256-268.

[29] P.R. Scheeper et. al., "Fabrication of Silicon Condensor Microphones using Single Wafer Technology", *Journal of Microelectromechanical Systems",* Volume 1, No. 3, page 147-154.

[30] D. Eichner and W. von Munch, " A two-step electrochemical etch-stop to produce freestanding bulk-micromachined structures", *Sensors and Actuators A,* Volume 60, page 103-107(1997).

[31] S.A. Campbell et. al., "Inhibition of pyramid formation in the etching of Si p<100> in aqueous potassium hydroxide-isopropanol", *Journal of Micromechanics and Microengg,* Volume 5, page 209-218 (1995).

# Vitae

**Santosh Pandey** was born on 18th September, 1976 in a city called Jamshedpur (India). He did his schooling in his home town after which he completed his Bachelors from Indian Institute of Technology, Kharagpur (India) in 1999. His Bachelors Degree was from the Department of Electronics and Electrical Engineering. He joined Lehigh University in the Department of Electrical Engineering and Computer Science with Prof. White as his advisor. He has been on Gotshell Fellowship and then on Sherman Fairchild Fellowship for the past two years. He completed the requirements for the Masters Program in 2001 after which he plans to continue his studies for the PhD Program from the same university. He has been a student member of the IEEE for the past two years and is also an associate member of the Sigma Xi Society.

END

OF

TITLE